Potential of High Spatial and Temporal Ocean Color Satellite Data to Study the Dynamics of Suspended Particles in a Micro-Tidal River Plume

Anouck Ody, David Doxaran, Quinten Vanhellemont, Bouchra Nechad,
Stefani Novoa, Gaël Many, François Bourrin, Romaric Verney, Ivane Pairaud,
Bernard Gentili

![remote sensing logo]

![MDPI logo]

Article

Potential of High Spatial and Temporal Ocean Color Satellite Data to Study the Dynamics of Suspended Particles in a Micro-Tidal River Plume

Anouck Ody [1,*], **David Doxaran** [1], **Quinten Vanhellemont** [2], **Bouchra Nechad** [2], **Stefani Novoa** [1], **Gaël Many** [3], **François Bourrin** [3], **Romaric Verney** [4], **Ivane Pairaud** [5] **and Bernard Gentili** [1]

[1] Laboratoire d'Océanographie de Villefranche sur Mer (LOV), UMR 7093, CNRS/UPMC, F-06230 Villefranche Sur Mer Cedex, France; david.doxaran@obs-vlfr.fr (D.D.); stefani.novoa@obs-vlfr.fr (S.N.); bernard.gentili@obs-vlfr.fr (B.G.)

[2] Royal Belgian Institute of Natural Sciences (RBINS), Operational Directorate Natural Environment, B-1200 Brussels, Belgium; qvanhellemont@naturalsciences.be (Q.V.); bnechad@naturalsciences.be (B.N.)

[3] Centre de Formation et de Recherche sur les Environnements Méditerranéens (CEFREM), UMR 5110, CNRS/UPVD, F-66100 Perpignan, France; gael.many@univ-perp.fr (G.M.); fbourrin@univ-perp.fr (F.B.)

[4] IFREMER, Centre Bretagne, Laboratoire de Dynamique Hydro-Sédimentaire, F-29280 Brest, France; Romaric.Verney@ifremer.fr

[5] IFREMER, Centre Méditerranée, Laboratoire Environnement Ressources Provence Azur Corse, F-83507 La Seyne sur Mer, France; Ivane.Pairaud@ifremer.fr

[*] Correspondance: anouck.ody@obs-vlfr.fr; Tel.: +33-493-763-738

Abstract: Ocean color satellite sensors are powerful tools to study and monitor the dynamics of suspended particulate matter (SPM) discharged by rivers in coastal waters. In this study, we test the capabilities of Landsat-8/Operational Land Imager (OLI), AQUA&TERRA/Moderate Resolution Imaging Spectroradiometer (MODIS) and MSG-3/Spinning Enhanced Visible and Infrared Imager (SEVIRI) sensors in terms of spectral, spatial and temporal resolutions to (i) estimate the seawater reflectance signal and then SPM concentrations and (ii) monitor the dynamics of SPM in the Rhône River plume characterized by moderately turbid surface waters in a micro-tidal sea. Consistent remote-sensing reflectance (Rrs) values are retrieved in the red spectral bands of these four satellite sensors (median relative difference less than ~16% in turbid waters). By applying a regional algorithm developed from *in situ* data, these Rrs are used to estimate SPM concentrations in the Rhône river plume. The spatial resolution of OLI provides a detailed mapping of the SPM concentration from the downstream part of the river itself to the plume offshore limits with well defined small-scale turbidity features. Despite the low temporal resolution of OLI, this should allow to better understand the transport of terrestrial particles from rivers to the coastal ocean. These details are partly lost using MODIS coarser resolutions data but SPM concentration estimations are consistent, with an accuracy of about 1 to 3 g·m^{-3} in the river mouth and plume for spatial resolutions from 250 m to 1 km. The MODIS temporal resolution (2 images per day) allows to capture the daily to monthly dynamics of the river plume. However, despite its micro-tidal environment, the Rhône River plume shows significant short-term (hourly) variations, mainly controlled by wind and regional circulation, that MODIS temporal resolution failed to capture. On the contrary, the high temporal resolution of SEVIRI makes it a powerful tool to study this hourly river plume dynamics. However, its coarse resolution prevents the monitoring of SPM concentration variations in the river mouth where SPM concentration variability can reach 20 g·m^{-3} inside the SEVIRI pixel. Its spatial resolution is nevertheless sufficient to reproduce the plume shape and retrieve SPM concentrations in a valid range, taking into account an underestimation of about 15%–20% based on comparisons with other sensors and *in situ* data. Finally, the capabilities, advantages and limits of these satellite sensors are discussed in the light of the spatial and temporal resolution improvements provided by the new and future generation

of ocean color sensors onboard the Sentinel-2, Sentinel-3 and Meteosat Third Generation (MTG) satellite platforms.

1. Introduction

Terrestrial substances transported by rivers into coastal seas directly affect nutrient availability, euphotic depths, phytoplankton productivity and transport of pollutants. They also represent an important component in the global carbon cycle [1] but are still poorly understood [2]. An operational monitoring of suspended particulate matter (SPM) concentrations in estuaries and river plumes is thus necessary to improve sediment transport and ecosystem modeling, with a final goal to prevent long-term damage to coastal waters. Fluxes of SPM at river mouths are spatially and temporally highly variable, with periods of high flooding events corresponding to high sediments supply, followed by periods of low discharge. These variations mainly depend on the river basin characteristics (see details in [3]), seasons (mainly precipitations) but also on currents and wind conditions at the river mouth and are usually only roughly estimated due to the lack of measurements.

When available, field measurements are expensive and specific to a time and/or geographical location and are thus not fully representative of the spatial (three-dimensional) and temporal dynamics of SPM in estuarine and/or river plume systems. The new capabilities of recent ocean color satellite sensors represent an efficient way to complement scarce field measurements and to monitor the surface transport of SPM through river mouths, in river plumes and estuaries (e.g., [4–13]). These sensors offer a good compromise between revisit time (about a daily revisit at mid-latitudes, depending on cloud cover) and spatial resolution (typically ranging from 250 to 1000 m). Most of them show a spectral resolution covering at least the visible and near-infrared (NIR) spectral regions required for atmospheric corrections of satellite data and estimation of SPM concentrations (e.g., [14,15]). Other satellite-borne sensors initially designed for land and/or meteorological applications, with at least red and NIR spectral bands, can also be used for monitoring SPM in coastal waters. The SPOT (Satellite Pour l'Observation de la Terre) and Landsat high spatial resolution sensors have proved their capabilities in mapping concentrations of suspended solids in highly turbid waters [13,16–18]. High temporal resolution satellite ocean color data acquired onboard geostationary satellite platforms has been demonstrated to provide valuable information in terms of SPM dynamics (e.g., [12,19,20]). A combination of these high temporal and high spatial resolution sensors should provide optimal remote sensing observations of surface SPM dynamics in coastal waters when operationally applied to data obtained by the next generation of (ocean-color) sensors: (i) MSI (MultiSpectral Instrument) and OLCI (Ocean and Land Color Instrument) onboard the Sentinel-2 and 3 (S-2 and S-3) polar-orbit platforms; and (ii) the Flexible Combined Imager (FCI) onboard the future Meteosat Third Generation (MTG) satellites.

Among current satellite sensors, we can list the ocean color sensor MODIS (Moderate Resolution Imaging Spectroradiometer) on board the polar-orbiting Aqua and Terra satellites, the Operational Land Imager (OLI) on the polar-orbiting Landsat-8 satellite and finally SEVIRI (Spinning Enhanced Visible and Infrared Imager) onboard the Meteosat Second Generation (MSG-3) geostationary platforms. The data recorded by these sensors cover the range of temporal (15 min to 1 day) and spatial (30 m to 3×5 km^2) resolutions currently available for the monitoring of SPM dynamics and are well designed to prepare the scientific exploitation of the next satellite sensors generation. The main objective of this study is to test and compare the capabilities and limits in terms of spectral, spatial and temporal resolutions of these three remote-sensing sensors (MODIS, SEVIRI and OLI) for the monitoring of SPM concentration in a river plume, here the Rhône River in the western Mediterranean Sea. This river is

the dominant source of freshwater and terrestrial substances in the Gulf of Lion [21] and generates a buoyant plume dominated by suspended sediments that strongly affect the coastal area near the river mouth [8]. The Rhône River plume is typical of moderately turbid waters, featured by a strong cross-shore gradient (typically from 40 $g \cdot m^{-3}$ to 1 $g \cdot m^{-3}$ or below), whose dynamics are mainly driven by winds and currents (e.g., [22–24]). This area is thus well-adapted to test sensors' capabilities in a micro-tidal coastal environment. Specific objectives are to test (i) the retrieval of the seawater reflectance signal and SPM concentrations and (ii) the capability of each sensor, in terms of spectral, spatial and temporal resolutions, to monitor the dynamics of SPM in such a river plume. In a first step, we test the capabilities of the three selected sensors, in terms of spectral resolution, to estimate SPM concentrations. Field measurements of SPM concentration and seaborne reflectance are used to establish, for each sensor, the best relationship between remote-sensing reflectance (Rrs, in sr^{-1}) and SPM concentrations in the Rhône River plume. Different spectral bands are tested. In addition, in the scope of combining sensors data, Rrs for each sensor are compared to each other to test their consistency. As a second step, we determine the impact of the spatial resolution of these three sensors on the retrieval and mapping of SPM concentrations. The capabilities and limits of each sensor are tested, first by progressively degrading high spatial resolution satellite data, then based on direct comparisons between satellite and *in situ* data. In a third step, we test the capabilities of the temporal resolution of the three sensors for the monitoring of SPM concentration variations and dynamics. Finally, we discuss the perspectives offered by the next generation of high resolution satellite sensors.

2. Materials and Methods

2.1. Study Area and Context

The study area is located in the north-western (NW) part of the Mediterranean Sea in the Gulf of Lion (Figure 1). This coastal region is one of the largest continental shelves of the Mediterranean Sea and is strongly affected by the inputs of the Rhône River, which is one of the major Mediterranean contributor in terms of liquid and solid discharges (e.g., [25]). The Rhône River is 812 km long originating in Switzerland and splitting into two branches, the Grand Rhône and Petit Rhône at Arles (south-eastern France), about 60 km upstream the river mouth. Based on [26], 80% of terrigenous material in the Gulf of Lion as well as 95% of the freshwater discharge [21] originate from the Rhône, with the "Grand Rhône" contributing to about 90% of this export to the coastal ocean.
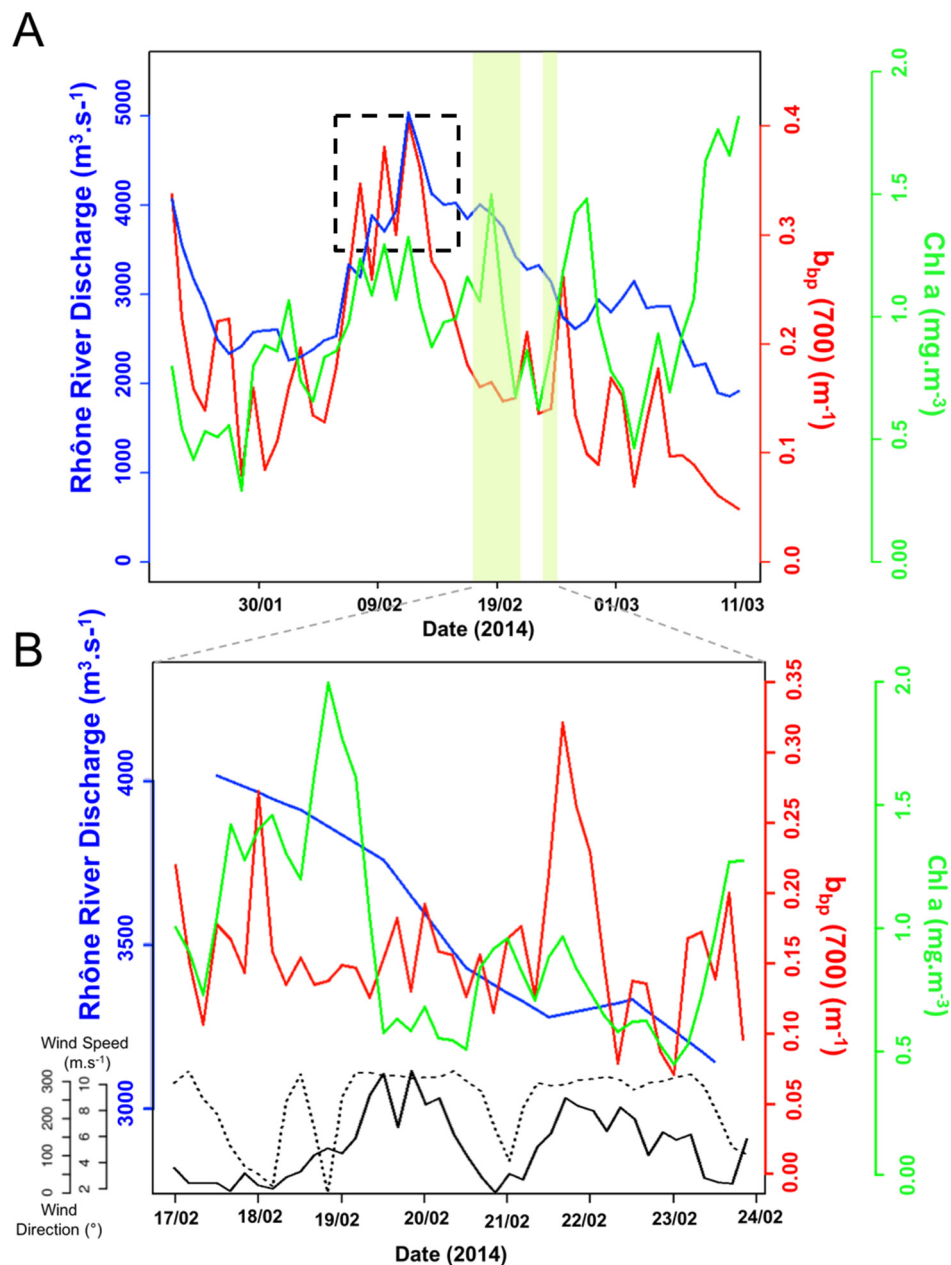
The Rhône River freshwater discharge is characterized by an annual mean value of 1700 $m^3 \cdot s^{-1}$ but shows strong seasonal and interannual variations due to variable climatic conditions along its drainage basin (one of the largest in Europe). It typically varies from less than 700 $m^3 \cdot s^{-1}$ in summer to more than 4000 $m^3 \cdot s^{-1}$ in spring and autumn and can exceed 10,000 $m^3 \cdot s^{-1}$ during exceptional peak flood events [25]. This freshwater discharge generates a buoyant surface plume characterized by high loads of fine sediment particles resulting in SPM concentrations commonly ranging from ~2–4 $g \cdot m^{-3}$ to more than ~40 $g \cdot m^{-3}$ depending on the season and the position within the plume (mouth *vs.* offshore) [8,27].

Because of low tidal amplitude (few tens of centimeters), the Rhône River plume usually dilutes slowly and can extend over hundreds of kilometers offshore making it easily detectable on ocean color satellite data (Figure 1). The surface plume shows morphological fluctuations, mainly in terms of orientation and offshore extent, depending on wind, freshwater discharge and large-scale circulation conditions [22–24]. Thereby, under a constant NW wind, the plume tends to be pushed offshore; by opposition, onshore winds direct the plume towards the coast. These horizontal fluctuations are associated with a strong vertical stratification that depends on freshwater discharge, as well as hydrological and hydrodynamic properties (temperature, salinity, currents, waves). The water column is commonly composed of three layers: a thin surface plume (<1 m thickness close to the river mouth), an intermediate plume formed by particles settling from the surface plume, and a Bottom Nepheloid Layer (BNL) due to both transport of particles and resuspension of sediments (e.g., [28]).
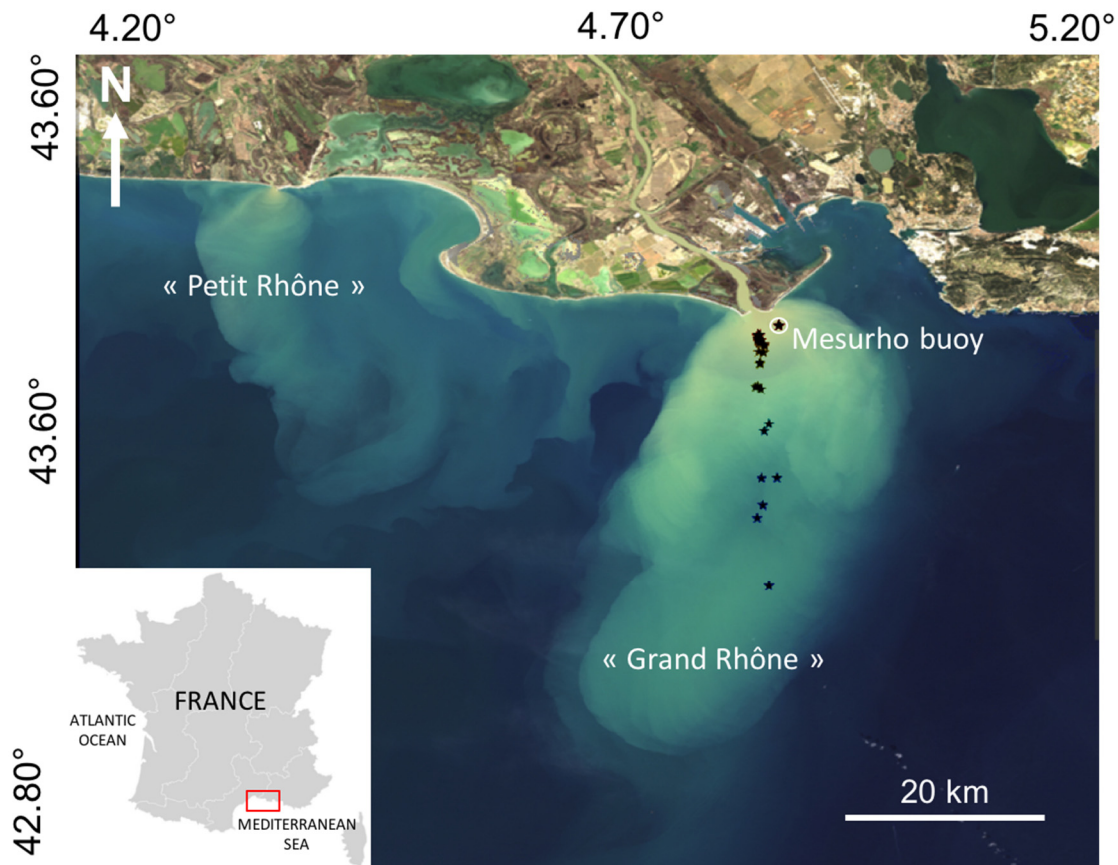
Figure 1. RGB georeferenced OLI image of the study area the 23 February 2014. Black stars locate the TUCPA field campaign stations (see Section 2.3 for details), the autonomous Mesurho station is indicated by a white circle.

In January 2014, an historical precipitation event resulted in several high flood events with the Rhône River freshwater discharge reaching up to 6000 $m^3 \cdot s^{-1}$. This study focuses on a period (17 to 23 February) starting during one of these flooding events, a few days after it reachs its maximum freshwater discharge (11 February, ~5000 $m^3 \cdot s^{-1}$ (Figure 2)). The freshwater discharge during this period ranged from 4000 to 3500 $m^3 \cdot s^{-1}$. This flooding event resulted in an increase of the surface SPM concentration in the vicinity of the river mouth (Figure 2), which then quickly decreased to reach a quasi-stable concentration during the study period (about 45–60 $g \cdot m^{-3}$ in the river mouth based on *in situ* gravimetric measurements). The chlorophyll-a (Chl-a) concentration was globally low (<2 $mg \cdot m^{-3}$, Figure 2) throughout the study period with some fluctuations mainly inversely correlated to SPM concentration variations. The Chl-a concentration started to drastically increase at the end of the flooding event when both the Rhône River discharge and SPM concentrations reached their low pre-flood level values (Figure 2).

Figure 2. (**A**) Rhône River freshwater discharge (blue) measured at Beaucaire-Tarascon (65 km upstream the Rhône River mouth) as well as particulate backscattering coefficient $b_{bp}(700)$ (as a proxy of SPM concentration [8]) (red) and Chl a fluorescence (green) measured by the Wetlabs ECO-BB2FL sensor at the Mesurho buoy, from the 22 January to the 11 March (daily averaged values). The $b_{bp}(700)$ coefficient was calculated from the light backscattering data measured at 117° and 700 nm ($\beta(117°,700)$) following the formula $b_{bp} = 2\pi \times 1.1 \times \beta(117°,700)$ [29] (water light backscattering and absorption losses were neglected). Dashed black rectangle indicate data that could be altered by probe saturation. Green zone indicates study period from 17 to 23 February; (**B**) Same for the period from 17 to 23 February 2014 (green zones on (**A**)) (data averaged over 4 h). Black solid line and black dashed lines represent 4 hours averaged wind speed and direction, respectively.

2.2. Autonomous Field Measurements

In 2009, a fixed (43°19.2′N/4°52′E) monitoring platform (Mesurho, http://www.ifremer.fr/medicis/projets/mesurho.html), equipped with subsurface and bottom sensors, was installed 2 km southeast of the Rhône River mouth (bottom depth of 20 m). Since then, it continuously records water

temperature, conductivity, turbidity and current velocity, among other parameters [30]. In addition, a bio-optical sensor was installed on the platform, at ~1 m depth, from 22 January 2014 to 11 March 2014 to record additional sub-surface *in situ* data (Figure 2). This Wetlabs ECO-BB2FL sensor measures light backscattering at 117° at the fixed wavelength of 700 nm ($\beta_{117}(700)$ in $sr^{-1} \cdot m^{-1}$) as well as chlorophyll fluorescence at a sample rate of 15 minutes (Figure 2). The measured $\beta_{117}(700)$ data (in $sr^{-1} \cdot m^{-1}$) was converted into the particulate backscattering coefficient ($b_{bp}(700)$, in m^{-1}) which is a robust proxy of the SPM concentration [8,29,31]. The $b_{bp}(700)$ coefficient was obtained through the formula $b_{bp}(700) = 2\pi \times 1.1 \times \beta_{p117}(700)$ [29], with $\beta_{p117}(700) = \beta_{117}(700) - \beta_{w117}(700) \sim \beta_{117}(700)$, as the water light backscaterring ($\beta_{w117}(700) \sim 10^{-5}$) is negligible compared to particulate light backscattering signal ($\beta_{p117}(700) \sim 10^{-2}$) in turbid waters. The $\beta_{117}(700)$ values were here not corrected for absorption losses (except for pure water absorption) as no absorption measurement was available for this dataset. However at 700 nm these absorption corrections typically correspond to less than 5% of the measured signal in the Rhône River plume [8]. The low overall Chl-a concentrations (<2 mg·m^{-3}) during the study period (Figure 2) suggest a total suspended particle matter dominated by mineral rather than organic matter. Consequently, the Chl-a concentration will not be considered in this study.

The Rhône River freshwater discharge was measured at a hydrometric station located in Beaucaire-Tarascon, about 65 km upstream the Rhône River mouth. Daily averaged data were exported from the Hydrologic data bank (http://www.hydro.eaufrance.fr/) for the period corresponding to the Mesurho data acquisition. Hourly (10 min burst average) wind direction and speed were measured at an altitude of 10 m at a meteorological station located on the coast at Cap-Couronne about 20 km east of the river mouth.

2.3. Field Bio-Optical and Biogeochemical Measurements

In the frame of the TUCPA (Coastal Turbidity and Autonomous Platforms) project, two oceanographic campaigns took place in the vicinity of the Rhône River mouth from 28 to 31 January and from 17 to 20 February 2014 onboard the Antédon II research vessel. This study focuses only on the second campaign where Rrs measurements were performed in addition to surface SPM concentrations.

2.3.1. Above-Water Hyperspectral Radiometric Measurements

Above-water hyperspectral radiometric measurements were carried out in 27 stations (Figure 1) to compute the Rrs signal. Measurements were performed with two radiance and one irradiance TriOS-RAMSES hyperspectral radiometers. The two radiance sensors were used to measure the total upwelling and sky radiances, respectively Lt and Ls ($W \cdot m^{-2} \cdot sr^{-1}$). The irradiance sensor was used to measure the downwelling irradiance signal (Ed, $W \cdot m^{-2}$). The radiance sensors were mounted on a frame hold manually above the air-sea interface with a solar relative azimuth angle around 135° (angle actually varying from 90° to 140° depending on light and sea-state conditions). The nadir and zenith angles of the sea- and sky-viewing radiance sensors were 40° as recommended by [32]. The irradiance sensor was hooked to a vertical mast at the front of the boat pointing the zenith and away from ship-induced shadow effects.

At each station, measurements were made during and after collection of a surface water sample. Radiometric measurements last 2 to 12 min, depending on the allocated time, taking simultaneous scans of the three instruments every 15 s. The sensors spanned the 350–950 nm spectral range with a spectral resolution of 3.3 nm. Data were recorded using a TriOS GmbH MSDA software using the most recent nominal calibration coefficients (set in 10/2014). Calibrated data for Ed, Lt and Ls were then interpolated to 1 nm intervals before processing.

The Rrs signal was computed from each simultaneous above water measurements of irradiance, Ed, total upwelling radiance, Lt, and sky radiance, Ls, as [32]:

$$R_{rs} = \frac{L_t - \rho L_s}{E_d} \tag{1}$$

where ρ is the air-water interface reflection coefficient. This coefficient may vary strongly with wind speed for clear sky conditions because of reflection of brighter parts of the sky in the case of higher waves [32], but is approximately independent of wind speed under overcast skies. This is accounted for by switching between clear sky and cloudy sky models for ρ, according to the ratio Ls/Ed at 750 nm (see Equations (23) and (24) in [33]).

For each of the 27 stations, the measured Rrs spectra were filtered, then averaged. As a first step, outlier spectra (*i.e.*, Rrs spectra for which either Ls, Lt or Ed spectrum differs by more than 25% the median spectrum at 550 nm) as well as spectra acquired with a ship inclination higher than $10°$ were removed. Then, the first seven spectra acquired during a period of stable illumination conditions, *i.e.*, irradiance (Ed) variations between two continuous spectra <15%, were selected. Finally, only spectra differing less than 15% from the median reflectance spectra were selected and averaged. Sea and sky conditions were rather stable during the campaign. These conditions and thresholds, especially those on the ship inclination ($10°$), were thus chosen in order to keep at least three spectra to be averaged per station, and with an acquisition time difference between Rrs measurements and SPM concentration sampling less than ~10 min. Moreover, different tests showed that whatever the conditions and the threshold, the impact was less than ~3% in the slope of the linear relationship between SPM concentrations and Rrs (see Section 3.1.1).

2.3.2. SPM Concentration and Turbidity Measurements

At each station, water samples were collected within the surface layer (0 to 1 m depth) using a horizontal Niskin bottle. SPM concentration was determined by filtering at low vacuum known volumes (V in m^3) of seawater through precombusted (450 $°C$) and pre-weighed (M_0, in g) glass-fiber filters (Whatman GF/F, 0.7 nominal pore size), as described in [34]. Each filter was then rinsed with Milli-Q water, and stored at ambient temperature on the ship and subsequently at $-80\ °C$ once back to the laboratory. At final processing, filters were dried for 24 h at 65 $°C$ then weighed (M, in g) under a dry atmosphere in order to obtain the SPM concentration:

$$SPM = \frac{(M - M_0)}{V}\left(g\ m^{-3}\right) \tag{2}$$

In addition to SPM concentration, the water turbidity was measured in triplicate for each sample using a portable HACH 2100Q turbidimeter following the protocol described in [35]. Turbidity values for each triplicate were then averaged.

The relationship between SPM and turbidity (not shown here) showed significant scatter likely resulting from the large diversity of particle composition and size along the river plume and from measurement uncertainties. Nevertheless, a linear relationship could be established with a coefficient of determination (R^2) of 0.60 and a slope of 0.88 (intercept fixed to 0) supporting that measured SPM concentrations are reliable enough for the global purpose of the present study.

2.4. Multi-Sensor Satellite Data

2.4.1. Data Specifications

Three satellite-borne sensors were considered:

1. OLI on the Landsat-8 polar-orbiting satellite,
2. MODIS an ocean color sensor aboard the polar-orbiting Aqua (MODIS-A) and Terra (MODIS-T) satellite platforms, and
3. SEVIRI, a meteorological sensor orbiting on the geostationary platform MSG-3.

The OLI sensor provides images with a temporal resolution of 16 days in 9 spectral bands in the visible, NIR and shortwave-infrared (SWIR) spectral regions with an approximate scene size of 170 (north-south) $\times$ 183 (east-west) km² and a spatial resolution of 30 m. In this study we only

considered spectral bands useful for atmospheric corrections and inversion of Rrs into SPM: the green (560 nm), red (655 nm) and NIR (864 nm) spectral bands, and the two SWIR bands (1601 nm; 2380 nm) [18]. MODIS-A and MODIS-T sensors provide both one image per day at the latitude of the study area (~43°N). MODIS sensors have 36 spectral bands with three spatial resolutions of 250 m, 500 m and 1 km, but only 5 bands are used for SPM retrieval: the two SWIR bands at 1240 and 2130 nm with a spatial resolution of 500 m (or NIR bands at 748, 869 nm with a spatial resolution of 1 km, depending of the selected atmospheric correction algorithm (e.g., [36])), the green band at 555 nm with a spatial resolution of 500 m and the red and NIR bands at 645 and 859 nm respectively with a spatial resolution of 250 m. SEVIRI provides data at a high temporal resolution with an image recorded every 15 min. Twelve spectral bands are available but only two can be used for SPM retrieval, the 635 nm spectral band (VIS0.6) used for SPM mapping and the 810 nm spectral band (VIS0.8) used for atmospheric corrections [19]. These spectral bands have a spatial resolution of 3 × 3 km at the sub-satellite point, but due to the latitude of the study area the pixel are elongated to ~3 × 5 km.

Spectral bands for these three sensors have close center wavelengths but their spectral band widths differ. They range from 20 to 75 nm for OLI and MODIS, and from 140 to 150 nm for SEVIRI.

All these sensors specifications are summarized in Table 1.

2.4.2. Satellite Dataset

The ocean color remote sensing dataset is composed of MODIS-A, MODIS-T, SEVIRI and OLI images acquired during the second TUCPA field campaign period (17 to 20 February 2014). Over this period, we focus only on observations acquired during the 17 and 20 February which are cloud-free days. As OLI data are only available on 23 February, MODIS and SEVIRI observations for this day are also included for comparison. Two MODIS observations per day are available, one in the morning between 09:50 and 10:55 UTC (MODIS-T), and one at noon between 12:10 and 13:10 UTC (MODIS-A). SEVIRI images every 15 min are available for the three days, from 08:00 to 16:00 UTC. Some SEVIRI images show clouds that mask the Rhône River plume and were manually excluded from the dataset. The OLI image was recorded on 23 February at 10:24 UTC. The final dataset is thus composed of 6 MODIS images, 91 SEVIRI images and 1 OLI image.

2.4.3. Satellite Data Processing

Level 1A MODIS-A and MODIS-T data were downloaded from the oceancolor.gsfc.gov website then processed using the SeaDAS (version 7.0) software (seadas.gsfc.nasa.gov) to generate geo-location and Level 1B files. Rrs(555), Rrs(645) and Rrs(859) Level 2 products were generated using the l2gen function. Four atmospheric corrections were tested to determine the most suitable for the moderately turbid waters of the Rhône River plume: (1) the MUMM [37]; (2) the NIR [38]; (3) the SWIR [39,40] and (4) the NIR-SWIR [36] atmospheric correction algorithms. The MUMM atmospheric correction algorithm is based on the spatial homogeneity of the water-leaving radiances and aerosols ratios (α and ε respectively, see Table 1) between two NIR bands (748 and 869 nm for MODIS sensors) [37]. This assumption is expected to be valid only in moderately turbid waters [18,37,41]. The NIR and SWIR atmospheric correction algorithms estimate the aerosol reflectance using NIR (748 nm and 869 nm) and SWIR (1240 and 2130 nm) MODIS bands respectively (Table 1), assuming that the water leaving reflectance is negligible at these wavelengths. These NIR and SWIR algorithms are respectively adapted to low and high turbid waters. The NIR-SWIR atmospheric correction algorithm [36,42] shifts between NIR and SWIR corrections based on a turbid water index and is thus adapted to both low and high turbid waters. As expected (but not shown here), the NIR correction tends to globally underestimate Rrs values in the Rhône River plume compared to other corrections. This is due to an overestimation of the aerosols reflectance because of a non-null water-leaving reflectance of moderately turbid waters in the NIR bands. The MODIS-A Rrs(645) products generated on 23 February 2014 using MUMM (1) and NIR-SWIR (4) atmospheric correction algorithms are compared in Figure 3A. Scatter-plots comparing the two Rrs products for the six available MODIS-A and -T images are also shown on Figure 3A

(bottom panel). The MUMM and NIR-SWIR atmospheric correction algorithms show consistent and quite similar results: a linear relationship is obtained between the two Rrs(645) products with a slope of 0.97 (23 February) and 0.99 (for the combined six dates) and a determination coefficients of ~0.97. Small differences are observed for high Rrs values (>0.015 sr^{-1}) where the MUMM algorithm shows higher Rrs values than the SWIR one (Figure 3A), leading to a relative difference between the two products of about 6% (median value) and maximum differences of 20% for the most turbid waters. This relative difference is minimum in the less turbid waters at the offshore limit of the plume but can increase up to 50% in the clearest waters out of the plume. The difference observed for high Rrs could be due to the fact that the MUMM correction is only adapted to moderately turbid waters. In [41], the authors showed that the main assumption in the MUMM algorithm (*i.e.*, a constant α) is only valid up to Rrs values of about 0.010 sr^{-1} at 748 nm and ~0.006 sr^{-1} at 869 nm. Beyond these values, Rrs(748) starts to saturate while Rrs(869) still linearly increases with turbidity and the relationship between Rrs(748) and Rrs(869) becomes non-linear. Based on *in situ* radiometric data (Section 2.3.1), Rrs at 748 and 869 nm varied in the range ~[0–0.014] sr^{-1} and ~[0–0.008] sr^{-1}, respectively, during the study period (from the river mouth to the offshore limit of the plume), so that the limit of validity of the MUMM algorithm was probably reached in the most turbid waters observed. However, on MODIS Rrs products generated for the study period using either NIR-SWIR or MUMM correction algorithms, only 1% of pixels exceed the limit given by [41], *i.e.*, the limit of validity of the MUMM atmospheric correction algorithm. Moreover, the non-linearity of the 748:869 nm ratio results in an overestimation of the atmospheric component by the MUMM algorithm (e.g., [18]) and then to an underestimation of the Rrs values. Rrs values exceeding the limit of validity of the MUMM correction should thus be underestimated and not overestimated compared to Rrs values corrected with the NIR-SWIR algorithm. The difference between MUMM and NIR-SWIR algorithm observed in Figure 3A is thus here attributed to the low Signal to Noise Ratio (SNR) of the MODIS SWIR bands, that prevents an accurate estimation of the aerosol reflectance and of the turbid water index in moderately turbid waters. As already noticed in previous studies (e.g., [43]), this results in rather noisy Rrs data. This is clearly observed in moderately turbid parts of the river plume (0.015 > Rrs > 0.025 sr^{-1}) (Figure 3A). In addition significant areas where data are missing due to atmospheric corrections failures are observed (grey areas in the left part of the plume on Figure 3A). The Rrs product generated using the SWIR atmospheric correction is not presented here but shows similar noisy Rrs values. Conversely, the MUMM atmospheric correction algorithm results in a homogeneous and well-defined Rrs product (Figure 3A). To summarize, the MUMM and NIR-SWIR atmospheric correction algorithms provide consistent Rrs(645) values but the MUMM algorithm gives a better quality product. The MUMM algorithm appears as the most appropriate method to correct for atmospheric effects MODIS data recorded over the moderately turbid waters of the Rhône River plume. This algorithm is selected for the rest of the present study even if match-ups are still needed for a concluding validation of the MUMM atmospheric correction algorithm especially for highest turbid waters (river mouth).

SEVIRI L1.5 data were obtained from the EUMETSAT website (eumetsat.int) and cropped to the North Gulf of Lion region (127 × 36 pixels). The water-leaving reflectance was obtained at the VIS0.6 band after correcting SEVIRI data for (1) atmospheric gas absorption; (2) Rayleigh scattering; (3) scattering by aerosols following the processing detailed in [19,20]. This atmospheric correction algorithm uses an approach similar to the MUMM correction [37] with the red (VIS0.6) and NIR (VIS0.8) bands of SEVIRI (called MUMM-S here after, see details in Table 1). [19] showed that this atmospheric correction is only valid for Rrs values lower than 0.02 sr^{-1} and 0.0038 sr^{-1} in the two red and NIR bands respectively. These limits are largely exceeded during the study period with Rrs values larger than 0.02 sr^{-1} in the SEVIRI red spectral band (see range of *in situ* radiometric data as shown by the SEVIRI red spectral band in Figures 4 and 5). This may likely result in an underestimation of the highest SEVERI derived Rrs values (see Section 3.1.2, Figure 6).

Table 1. Main characteristic of studied satellite sensors OLI, MODIS and SEVIRI and dataset.

| Sensor/Satellite		OLI/Landsat-8			MODIS/AQUA/TERRA			SEVIRI/MSG-3		
Spatial Resolution		30 m			250 m/500 m/1 km			3 × 5 km (at ~44°N)		
	Total	9			36			12		
Spectral Resolution (nm)	Used for SPM retrieval and atmospheric correction (A)	Band	Wavelength range (nm)	SNR [44]	Band	Wavelength range (nm)	SNR [45]	Band	Wavelength range (nm)	SNR [46]
		3 (Green)	525–600	296	4 (Green)	545–565	228			
		4 (red)	630–680	222	1 (Red)	620–670	128	VIS0.6 (Red)	560–710	>10.1
		5 (NIR)	845–885	199	2 (NIR)	841–876	201	VIS0.8	740–880	>7.3
		6 (SWIR1, A)	1560–1660	261	15 (NIR1, A)	743–753	586	(NIR,A)		
		7 (SWIR2, A)	2100–2300	326	16 (NIR2, A)	862–877	516			
					5 (SWIR1,A)	1230–1250	74			
					7(SWIR2, A)	2105–2155	110			
Temporal Resolution		16 days			1 day			15 min		
Atmospheric Correction Algorithm		SWIR [18] 1609, 2201 nm Spatially constant ε (Fixed aerosol type), determined for each image.			MUMM [37] 748, 869 nm α = 1.945 ε = 1.0 (fixed aerosol type)			MUMM-S [19,20] 635, 810 nm α = 6.09 ε = Spatially constant ε (Fixed aerosol type), determined for each image.		
Available observations over the studied period		1 (23/02/2014 10:24)			12 (T 17/02/2014 10:25; A 17/02/2014 12:10; T 20/02/2014 10:55; A 20/02/2014 12:40; T 23/02/2014 09:50; A 23/02/2014 13:10)			91 (17/02/2014 08:00 to 16:00; 20/02/2014 08:00 to 14:00; 23/02/2014 08:00 to 16:00)		
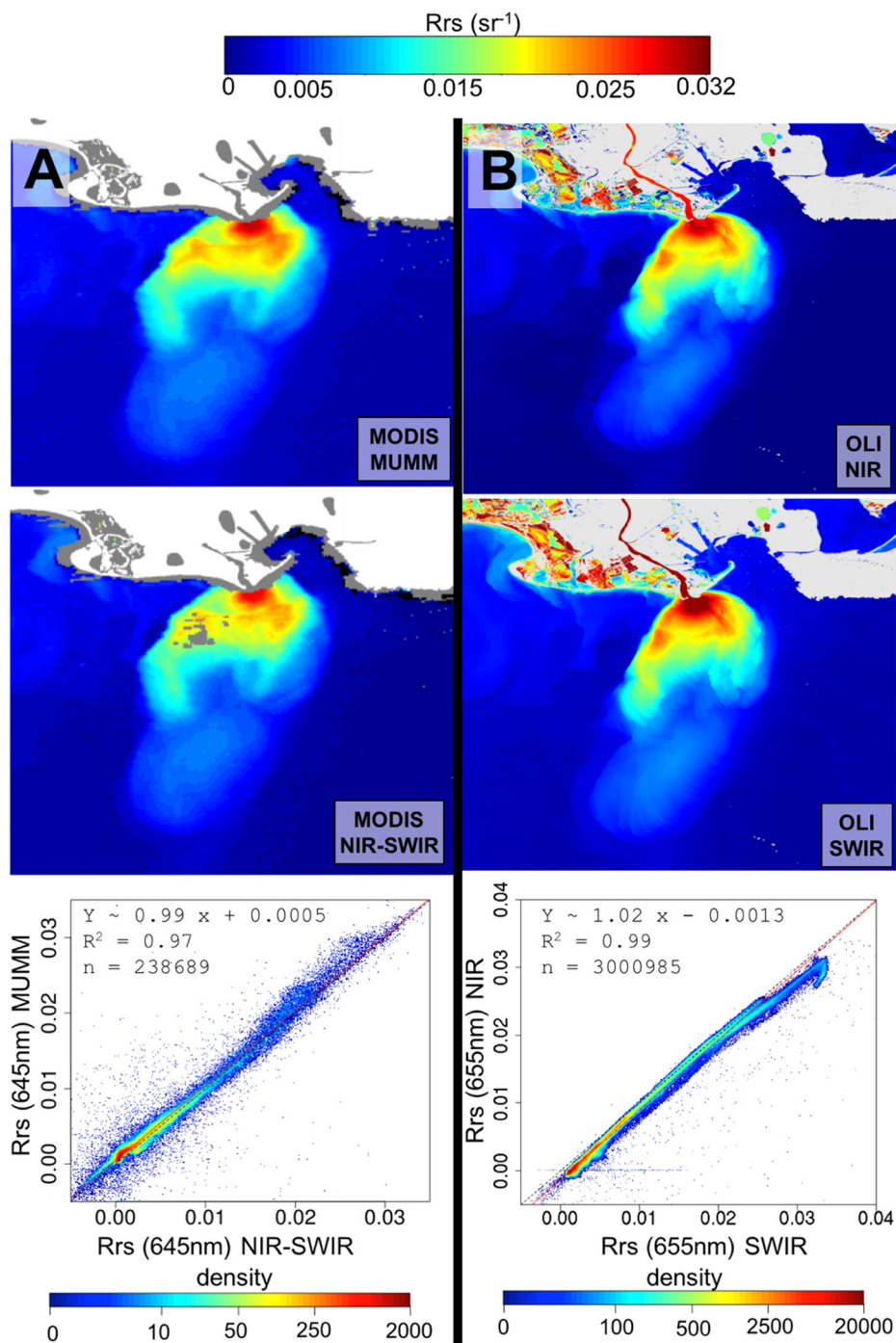
Figure 3. (**A**) MODIS-A Rrs(645) product of the Rhône River plume for the 23 February 2014 obtained using MUMM [37] (top) and NIR- SWIR [36,42] (middle) atmospheric corrections. Grey areas on the western part of the plume on the MODIS-A Rrs product obtained with the NIR-SWIR correction correspond to area flagged because of atmospheric correction failures. Scatter-plot on bottom panel is obtained by comparing the six available MODIS (-A and -T) Rrs(645) products corrected with both (MUMM and NIR-SWIR) atmospheric correction algorithms; (**B**) OLI Rrs(655) product of the Rhône River plume for the 23 February 2014 obtained using NIR [13] (top) and SWIR [18] (middle) atmospheric correction for OLI. Scatter-plot on the bottom panel are obtained by comparing OLI Rrs(655) product corrected with both (NIR and SWIR) atmospheric corrections algorithm. Colors on scatter plots denote pixel density.
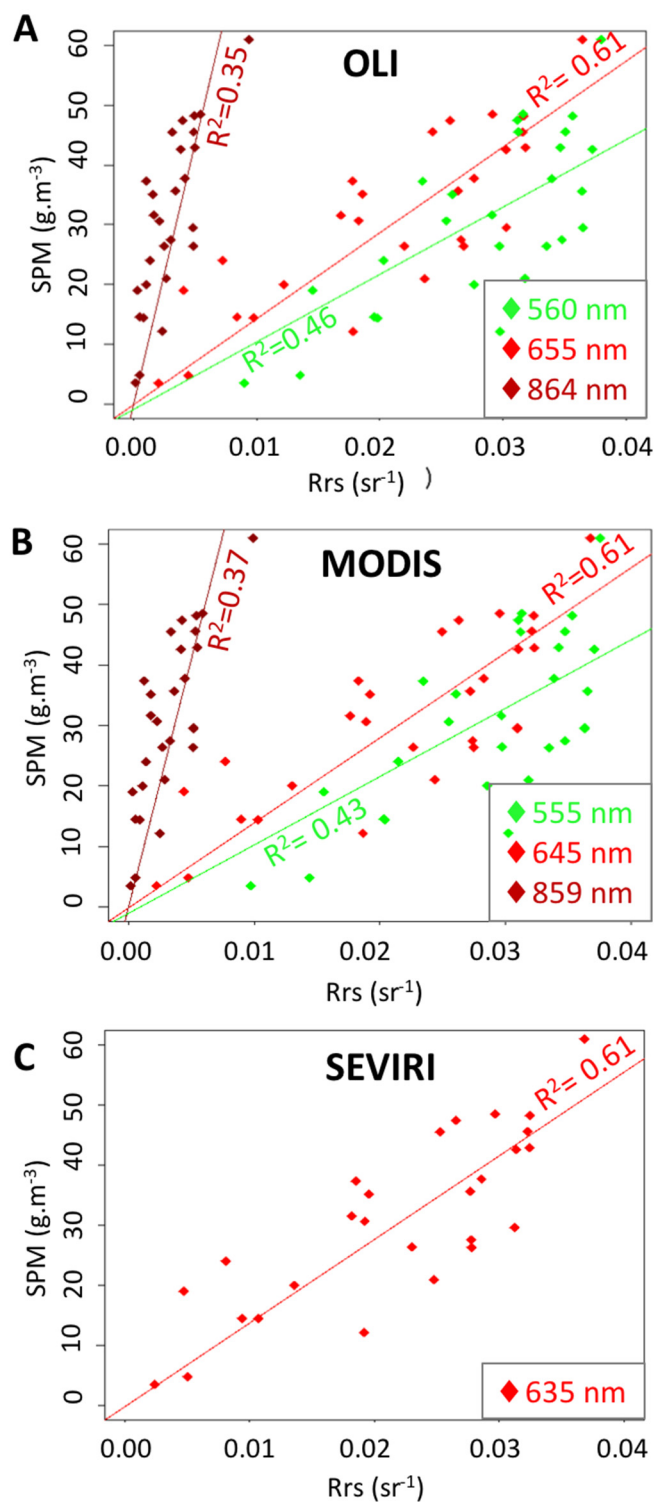
Figure 4. *In situ* Rrs weighted by sensitivity of red, green and NIR sensors spectral bands *vs. in situ* SPM concentration measured during the TUCPA campaign (27 stations) for the three sensors: (**A**) OLI; (**B**) MODIS -A and -T; (**C**) SEVIRI.

Orthorectified and terrain corrected Level 1T OLI data was obtained from the Landsat-8 portal on ESA website (https://landsat8portal.eo.esa.int/portal/) then processed using the ACOLITE software (http://odnature.naturalsciences.be/remsem/acolite-forum/) [13,18] to obtain water-leaving reflectances. Two atmospheric correction algorithms are proposed in ACOLITE: the NIR algorithm [13]

based on the MUMM approach and using the red (655 nm) and NIR (865 nm) bands, and the SWIR algorithm [18] using the high quality SWIR bands of OLI. Figure 3B shows that these two algorithms give consistent Rrs(655) products at low and medium Rrs values. At high Rrs (>0.02 sr^{-1}) differences between the two corrections increase. Highest Rrs values found in the vicinity of the river mouth and in the Rhône River are significantly underestimated by the NIR correction compared to the SWIR one. This clearly illustrates the limit of the NIR correction based on the assumption of a constant marine reflectance ratio in the NIR and emphasizes the advantages of high quality SWIR bands for atmospheric corrections even over moderately turbid waters [18]. The SWIR correction was thus applied to OLI data (see details in Table 1).
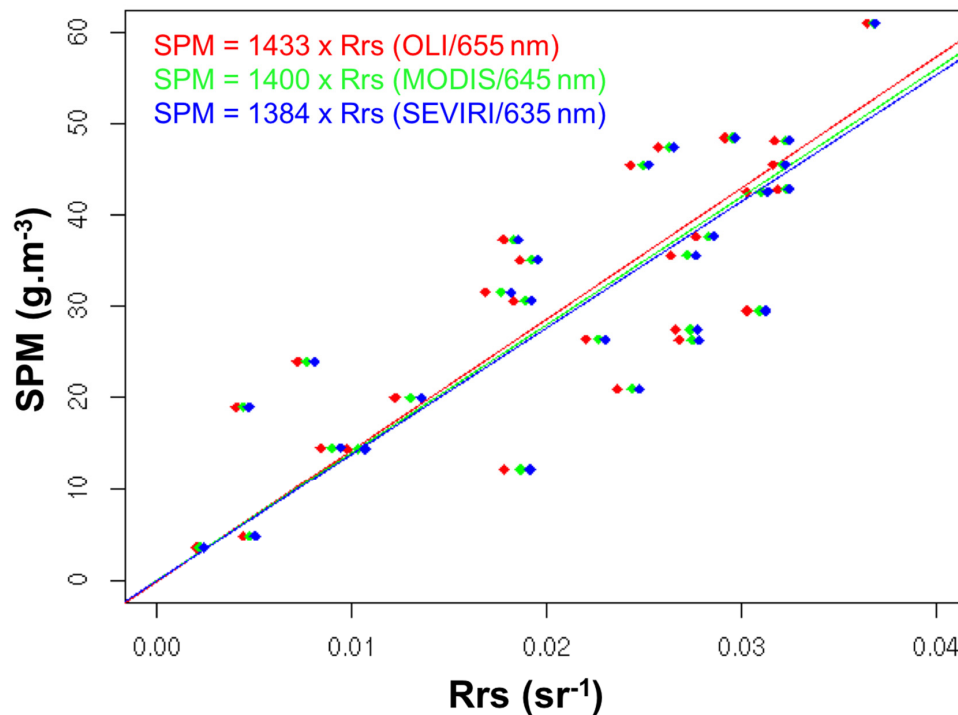
Figure 5. Empirical relationships between *in situ* Rrs (weighted by sensors spectral sensitivity) in the red spectral bands of the OLI (red), MODIS (green) and SEVIRI (blue) sensors and *in situ* SPM concentration obtained from TUCPA campaign measurments (27 stations). Three relations are very similar and show a correlation coefficient $R^2 \sim 0.61$.

For SEVIRI and OLI images, Rrs values were obtained by dividing the water-leaving reflectance by $\pi \, \text{sr}^{-1}$.

3. Results and Discussion

3.1. Impact of Satellite Sensor Spectral Resolution and Radiometric Characteristics on the Retrieval of SPM Concentration

Satellite sensors have different spectral resolutions (number of spectral bands, and bandwidth) that may be more or less suitable for the retrieval and mapping of SPM concentration. Moreover, data processing, spectral band wavelength range as well as radiometric characteristics (e.g., SNR, sensitivity) and radiometric calibrations differ from one sensor to another. This can induce differences in Rrs and SPM concentration values derived from data recorded by the different sensors. Here we first use radiometric and gravimetric *in situ* data to simulate Rrs in the spectral bands of each sensor in order to determine the best relationship between Rrs and SPM concentration, *i.e.*, to determine the spectral bands that are the most sensitive to variations of SPM within the concentration range

encountered in the study area. Then we intercompare Rrs data obtained in the selected spectral band for each sensor in order to test their consistency and assess their differences.

3.1.1. Best *In Situ* Based Rrs *vs.* SPM Regional Relationships for OLI, MODIS and SEVIRI

The Rrs signal is expected to increase with increasing SPM concentration then to saturate at high SPM concentrations. This saturation first occurs at short (blue, green) visible wavelengths then in the red spectral region (at about 10 and 50 g·m^{-3} at 555 and 645 nm, respectively) [15,16,47] and even in the NIR for extremely high SPM concentrations [48]. Depending on the SPM concentration range, Rrs variations within green, red or NIR spectral bands may be more sensitive, hence appropriate for the retrieval of SPM concentration [14,15,49]. The Rhône River plume is typical of moderately turbid waters with SPM concentrations ranging from 1 to more than 50 g·m^{-3} ([8], this study). Therefore, the three spectral bands (green, red and NIR) could be suitable for SPM concentration retrieval. *In situ* hyperspectral Rrs measurements from the TUCPA campaign dataset have been weighted by the spectral sensitivity of sensor spectral bands to obtain the equivalent Rrs values in the green, red and NIR spectral bands of the OLI, MODIS and SEVIRI satellite sensors (or only red for SEVIRI). The central wavelengths of the selected spectral bands are: 560 nm, 655 nm and 864 nm for OLI, 555 nm, 645 nm and 859 nm for MODIS, and 635 nm for SEVIRI. Empirical relationships were then established between Rrs in each sensor spectral bands and the corresponding *in situ* SPM concentration (Figure 4). The resulting relationships between Rrs and SPM are quite similar for the three sensors. Within the SPM concentration range sampled during the TUCPA field campaign (3–60 g·m^{-3}), the Rrs signal increases linearly with increasing SPM concentration in the red and NIR bands (Figure 4). The red band is however about five times more sensitive to SPM concentration variations than the NIR one: Rrs values range from ~0.002 to ~0.035 sr^{-1} in the red band and only from ~0.001 to ~0.007 sr^{-1} in the NIR one. A better linear correlation is obtained in the red spectral band (R^2 ~ 0.61 for the three sensors) than in the NIR band (R^2 ~ 0.35). In the green band, Rrs linearly increases with SPM concentration until about 30 g·m^{-3} (R^2 ~ 0.54 for SPM < 30 g·m^{-3}) then tends to saturate (Figure 4), precluding its use to estimate high SPM concentration values.

Based on these results, a simple linear relationship using the red band of each satellite sensor appears as the most robust and accurate option to invert Rrs into SPM concentration in the moderately turbid waters of the Rhône River plume. These results are supported by previous studies that showed that algorithms using one single band to estimate SPM concentration provides satisfactory results [15,17,50]. Results obtained by [15] also demonstrate that the optimal spectral band for SPM concentration estimation is situated in the red/NIR (680–730 nm) spectral region for concentrations ranging from 1 to 100 g·m^{-3}. Moreover, a simple linear relationship based on Rrs in the red spectral band shows advantages in the framework of this study: (i) the red band is the only one available for the three sensors and allows to obtain very similar relationships for the three of them (Figure 5); and (ii) the MODIS red band has the highest spatial resolution of 250 m. Authors in [8] also used a relationship based on the Rrs signal in the red wavelength range to estimate SPM concentration from the MODIS and MERIS (Medium Resolution Imaging Spectrometer) satellite sensors. However, to improve the relationship, the Rrs in the red band is multiplied by a ratio between the green and blue band Rrs signals. This relationship was tested on TUCPA field campaign dataset. It also varies linearly with SPM concentration but the linear regression shows a lower R^2 of 0.56 compared to using the red band only. Moreover, a three bands relationship cannot be applied to SEVIRI data as only the red band is available, and would decrease the spatial resolution of MODIS to the 500 m resolution of its green and blue spectral bands. The three best relationships between *in situ* Rrs (sr^{-1}) and SPM concentration (g·m^{-3}), obtained in the red spectral bands of the three satellite sensors OLI, MODIS and SEVIRI are presented on Figure 5 and reported hereafter:

$$\text{SPM} \ = \ 1433 \times \text{Rrs} \,(\text{OLI}/655\,\text{nm}) \quad \text{R}^2 \ = \ 0.615 \tag{3A}$$

$$\text{SPM} \; = \; 1400 \times \text{Rrs} \, (\text{MODIS}/645 \, \text{nm}) \quad \text{R}^2 \; = \; 0.612 \tag{3B}$$

$$\text{SPM} \; = \; 1384 \times \text{Rrs} \, (\text{SEVIRI}/635 \, \text{nm}) \qquad \text{R}^2 \; = \; 0.610 \tag{3C}$$

The intercepts of the linear regressions should be fixed so that Rrs is equal to the reflectance of pure seawater (Rrs$_w$) when the SPM concentration is 0. Rrs$_w$, through the formula Rrs$_w$ = $\Re f/Q$ × $b_{bw}/(a_w + b_{bw})$ from [51,52], depends on the pure seawater inherent properties (absorption (a_w) and backscattering (b_{bw}) coefficients), on the Sun and viewing angles through the ratio $\Re f/Q$ which also accounts for bidirectional and reflexion-refraction effects at the air-water interface [51,52]. Relationships for the three sensors were computed for different intercepts calculated for different Rrs$_w$ values corresponding to solar and sensor zenith angles varying from 0° to 75°. The resulting values of the intercept vary between −0.065 and −0.18 (g·m^{-3}) that introduced a difference less than 1% on the estimated SPM concentration. Given the low impact of the intercept value on the SPM estimation in the relatively turbid waters of the Rhône River, and given the large range of solar and sensor zenith angles spanned by the three sensors, the intercepts in Equations (3A)–(3C) were set to 0. The resulting relationships (Equations (3A)–(3C)) show a significant scatter (R^2 of ~0.61) that can be explained by (i) the difficulty to measure in the field the SPM concentration within the thin Rhône River plume, *i.e.*, a less than 1 m thick turbid surface layer floating over underlying layers; (ii) the natural variations of SPM composition and size distribution along the river plume where different types of suspended particles (mainly sediments) mix and form aggregates in the presence of organic matter (e.g., [8,53]) and (iii) measurement uncertainties. Nevertheless, these relationships are more robust than those proposed by [54] as they are based on a larger range of SPM concentrations (3–60 g·m^{-3} in this study compared to 1–10 g·m^{-3} in [54]) and show a slightly better determination coefficient (R^2 of 0.61 for this study compared to 0.56 in [54]). These relationships should be improved in the future with the acquisition of supplementary *in situ* data. First, the acquisition of new *in situ* data at low SPM concentration should increase the robustness of these relationships at low Rrs and SPM concentration signal. Secondly, based on the TUCPA dataset, these relationships seem linear up to 60 g·m^{-3}, but more points at low and high SPM concentrations are needed to confirm this linearity. As proposed by [15], a non-linear relationship should be considered. In addition, the MODIS and OLI green bands may be used to better detect and quantify low SPM concentrations (<10 g·m^{-3}). For the purpose of the present study, the linear relationships established for each sensor (Equations (3A)–3C)) are considered as satisfactory.

3.1.2. Impact of Sensors Radiometric Characteristics on Rrs and SPM Retrieval

The Rrs product derived from the three satellite sensors depends on marine reflectance, but is also affected by the corrections applied to data recorded at the top of the atmosphere (e.g., atmospheric and bidirectional effects), the radiometric characteristics of the sensor spectral bands (*i.e.*, wavebands spectral range, SNR, sensitivity) and the radiometric calibration that are specific to each sensor. To account for these effects, we have compared Rrs products derived from data recorded by the red band of the four sensors: MODIS-A, MODIS-T, OLI and SEVIRI (Figure 6) (Note that from here Rrs corresponds to Rrs in the red band of each satellite sensor). To remove effects of the different sensors spatial resolutions, Rrs products from each sensor are reprojected into the same resolution (the coarser one) before comparison. Comparisons with SEVIRI are made over the whole study area (*cf.* Figure 1). To minimize differences due to the natural dynamics of the plume between SEVIRI and other data acquisition times, SEVIRI Rrs products preceding and following the MODIS-A, MODIS-T and OLI acquisition times are weight-averaged before comparison. The time difference between OLI and MODIS-T on 23 February is 35 min but is higher than 2 h with MODIS-A. Because of this large time difference, MODIS-A and OLI Rrs products were compared considering only a polygon inside the river plume, where Rrs variations are less important than in the plume boundaries regions. For a better comparison, the same polygon is used for the comparison between Rrs derived from MODIS-T and OLI. Nevertheless, we can notice that scatter-plots on Figure 6 show a scatter that increases with the time difference between sensor observations. This suggests that differences

dues to the natural dynamics of the plume are not totally removed. In order to take into account only the systematic differences due to sensor characteristics we here considered median relative differences values. Figure 6 shows that all sensors exhibit quite similar results with Rrs values well linearly correlated ($R^2 > 0.89$). Nevertheless, some differences are observed. As already reported by [12], SEVIRI tends to globally underestimate Rrs values compared to MODIS-A (Figure 6A) with Rrs (SEVIRI) $\approx 0.83 \times$ Rrs (MODIS-A). The median relative difference is about 16% in the moderately turbid waters of the Rhône River plume (Rrs > 0.01 sr^{-1}). It can increase to more than 50% in the less turbid waters (Rrs < 0.010 sr^{-1}) mainly found offshore. The difference between Rrs derived from SEVIRI and MODIS-T is smaller. The linear regression slope is close to 1 and the median relative difference is about 6% for high Rrs values (Rrs > 0.010 sr^{-1}) retrieved using these two sensors. Figure 6B shows that MODIS-T tends to overestimate low Rrs values (Rrs < 0.010 sr^{-1}) but to underestimate high Rrs values (Rrs > 0.010 sr^{-1}) compared to OLI. The median relative difference is about 7% in moderately turbid waters (Rrs > 0.010 sr^{-1}) but increases for the highest Rrs values observed around the river mouth ($>\sim0.025$ sr^{-1}) where it can reach 16%. The comparison between Rrs derived from OLI and MODIS-A shows a significant scatter mainly caused by the large acquisition time difference between the two images (Figure 6C). Nevertheless, Rrs values from the two sensors are linearly correlated with a slope of 1.01. As with MODIS-T, the median relative difference between Rrs derived from OLI and MODIS-A increases for the highest Rrs values (Rrs > 0.025 sr^{-1}) but remains less than 9%. As between SEVIRI and MODIS, the relative difference between OLI and MODIS-A and -T Rrs products in the less turbid waters (Rrs < 0.010 sr^{-1}, *i.e.*, mainly outside the plume) can reach more than 50% (not shown in Figure 6 because of the restriction of the comparison to a polygon inside the plume). Rrs values derived from SEVIRI are shifted by a constant offset towards lower values compared to Rrs derived from OLI (Figure 6D). This leads to SEVIRI Rrs values globally lower by about 6% in moderately turbid waters (Rrs > 0.010 sr^{-1}) and by more than 50% in the less turbid waters (Rrs < 0.010 sr^{-1}) compared to OLI Rrs values.

Part of these differences can be explained by the different spectral ranges of the sensors red band (Table 1) which leads to a small shift in Rrs values derived from OLI, MODIS and SEVIRI as clearly illustrated in Figure 5. To quantify this effect, we compared *in situ* Rrs simulated in the red band of each sensor (weighted by the red band spectral sensitivity, see Section 3.1.1 and Figure 5). Comparison shows that Rrs are well linearly correlated ($R^2 = 0.999$) with a slope close to 1 ($\pm 10^{-2}$) and a rather negligible intersect ($< 10^{-3}$ sr^{-1}). Nevertheless, this leads to a maximum relative difference between Rrs derived from SEVIRI red band (635 nm) and Rrs derived from OLI red band (655 nm) of about 16% for low Rrs values (Rrs < 0.010 sr^{-1}). This difference decreases down to 5% for the highest Rrs values observed in the river mouth. Similarly, the difference between Rrs derived from OLI and MODIS is less than 8% for low Rrs values and less than 3% for high Rrs values, and the difference between MODIS and SEVIRI Rrs is less than 9% for low values and less than 2% for high values. The differences in Rrs induced by the different red band spectral ranges of the three sensors are thus less than 5% in the moderately turbid waters of the river plume. The comparisons presented in Figure 6 were made after wavelength-shifting the Rrs values of the two compared sensors to the same spectral range (by applying a factor derived from *in situ* Rrs data comparison, see above), but no significant change were observed. This difference in spectral range cannot explain the differences observed in Figure 6. Note that SPM concentration is not affected by this effect as the Rrs *vs.* SPM concentration relationship is adapted to each sensor red band (see Section 3.1.1).
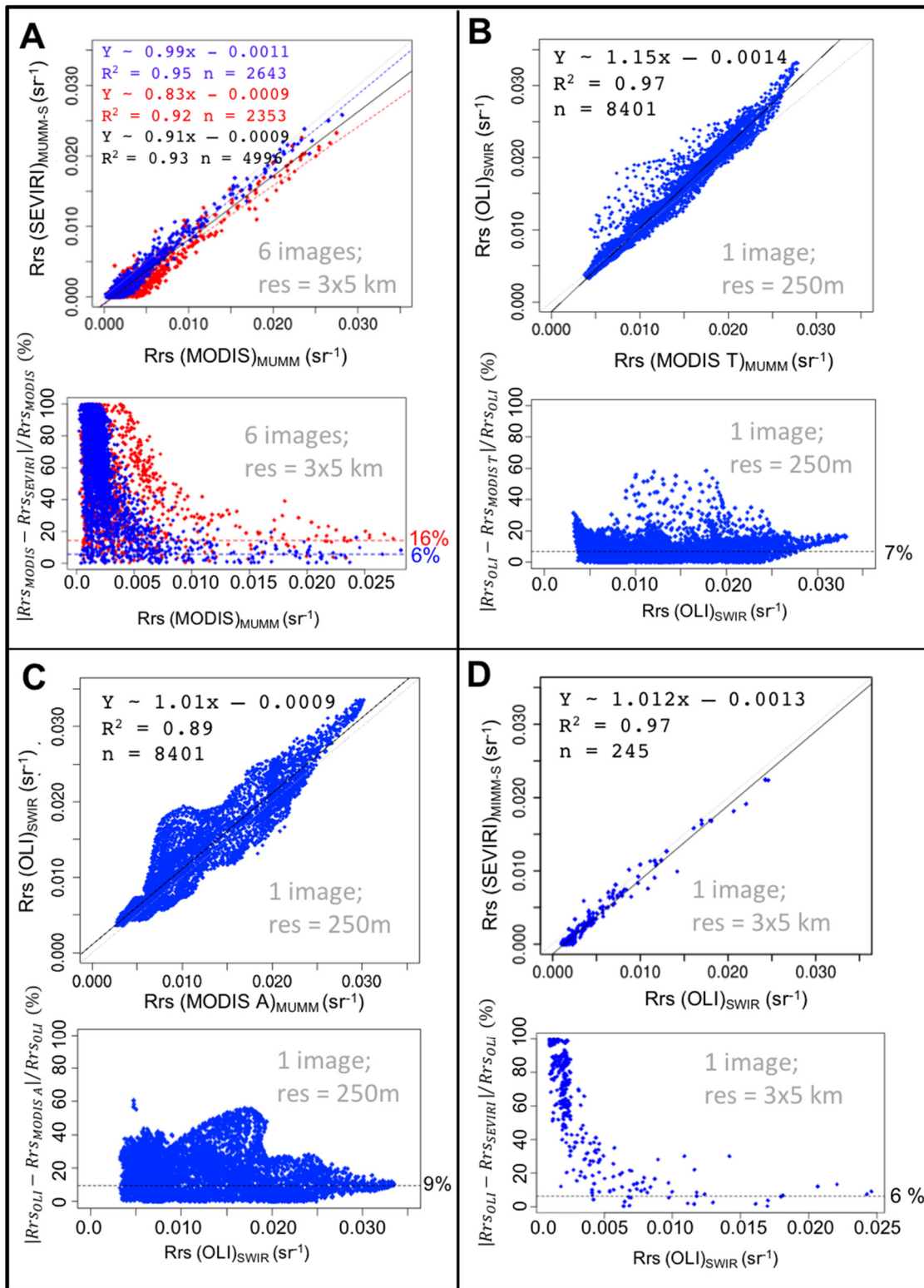
Figure 6. Intercomparison of Rrs obtained in the red spectral band of each satellite sensor. Scatter-plots (top) and relative differences (bottom) are shown for comparison between (**A**) SEVIRI and MODIS-A and −T; (**B**) OLI and MODIS-T; (**C**) OLI and MODIS-A; (**D**) OLI and SEVIRI. Because of the large time difference between MODIS-A and OLI data acquisitions, the corresponding Rrs products were compared considering only a polygon inside the river plume, where Rrs variations are less important than in the plume boundaries regions. For a better comparison, the same polygon is used for the comparison between Rrs derived from MODIS-T and OLI. Linear regressions are applied on each scatter plot, showing good correlation between all sensors. The median relative difference was calculated for Rrs > 0.010 (sr^{-1}) corresponding to Rrs observed in the moderately turbid waters of the Rhône River plume, and indicated by horizontal bars. The number of observations as well as the spatial resolution used for comparison are indicated in each plot.

Differences observed in Figure 6 can be partly caused by the atmospheric corrections applied, which are different for each sensor. This can particularly explain the underestimation of high Rrs values (Rrs > 0.025 sr^{-1}) by MODIS-A and -T compared to OLI. As previously discussed in Section 2.4.3., the use of NIR spectral bands in the MUMM atmospheric correction applied to MODIS data may lead to underestimation of the Rrs signal in highly turbid waters where the SWIR atmospheric correction applied to OLI is better suited. This is supported by the fact that this difference disappears when comparing MODIS-A Rrs with OLI Rrs values corrected by the NIR atmospheric correction instead of the SWIR correction. The difference between high Rrs values derived from OLI and MODIS-T is minimized when comparing MODIS-T with OLI data corrected by the NIR atmospheric correction but does not totally disappear. This remaining difference as well as the difference between MODIS-A and MODIS-T could be attributed to a degradation of the sensitivity and/or radiometric calibration of MODIS-T because of aging [55]. As proposed by [12], the different atmospheric corrections applied to MODIS and SEVIRI data, *i.e.,* the use of red and NIR bands for SEVIRI instead of two NIR bands for MODIS in the MUMM atmospheric correction algorithm, may explain the overall lower Rrs values obtained with SEVIRI compared to those obtained with MODIS-A. The lower radiometric sensitivity of SEVIRI can be an additional/alternative explanation [12]. Atmospheric corrections and the low sensitivity of SEVIRI can also be invoked to explain the shift between SEVIRI- and OLI-derived Rrs. Note also that bidirectional effects [51,56] are not taken into account in the processing of OLI and SEVIRI data, and could be an additional/alternative origin of differences between sensors-derived Rrs. It should also be noted that the differences observed between Rrs derived from OLI and Rrs derived from MODIS or SEVIRI have to be considered with caution as only one OLI image is considered in the present study.

To summarize, MODIS-A and OLI Rrs products are consistent except for the highest Rrs values (>0.025 sr^{-1}) where Rrs derived from MODIS are underestimated, likely because of an overcorrection for atmospheric effects by the MUMM atmospheric correction algorithm. Similarly, SEVIRI and MODIS-T show very close Rrs values but both are underestimated compared to Rrs derived from OLI and MODIS-A. Median relatives differences never exceed 16% in moderately turbid waters (Rrs > 0.01 sr^{-1}), which is satisfactory in the scope of combining the Rrs and SPM products from these different sensors (e.g., [12]). In waters with low SPM concentrations, the water-leaving signal is low and even negligible in the red spectral region. Combined with the different SNR of the considered satellite sensors, this certainly explains the larger differences observed between sensor Rrs products in these waters (Rrs < 0.010 sr^{-1}).

3.2. Impact of Satellite Spatial Resolution on the Retrieval and Mapping of SPM Concentration

Spatial resolution of satellite sensors determines the level of details observed on SPM maps, as well as the degree of accuracy and reliability of SPM concentrations derived from the Rrs signal with respect to *in situ* data. In the next section, we first try to predict the impact of spatial resolution on SPM mapping using the high spatial resolution satellite data of OLI, degraded at various lower spatial resolutions. Results are then compared to true OLI, MODIS and SEVIRI data at their native spatial resolution. Finally, the accuracy and reliability of Rrs and SPM products derived from meter to kilometer scales satellite sensor pixels are evaluated based on match-ups between satellite and *in situ* data.

3.2.1. Impact of Satellite Spatial Resolution Simulated Using OLI Data

In order to assess the impact of satellite spatial resolution on SPM estimation and mapping, we simulate satellite data at various spatial resolutions by degrading the 30 m resolution OLI image to coarser resolutions of MODIS and SEVIRI data. This allows isolating the effects of spatial resolution with respect to other parameters affecting the retrieval of Rrs and SPM concentration (see Section 3.1.2). Figure 7A shows the OLI-derived SPM product over the Rhône River plume area (23 February 2014) at OLI native spatial resolution (30 m), as well as averaged into coarser grids corresponding to MODIS

(250 m, 500 m and 1 km) and SEVIRI (3×5 km^2) spatial resolutions. A zoom on the Rhône River mouth, a region of particular interest for the estimation of fluxes of terrestrial substances exported by the river into the coastal ocean, is also presented in Figure 7A (right). This figure shows that the OLI SPM product at native resolution (30 m) provides a detailed view of the Rhône River plume and mouth with well apparent small-scale turbidity features. Pixels are also observed into the river itself (Figures 1 and 7A) suggesting that the OLI high resolution is well adapted to estimate and map SPM concentrations in the Rhône River plume, but also in the downstream part of the river (Figure 7A). This is well illustrated on Figure 7C where variations of SPM concentrations are well captured on the OLI image along a transect from the downstream part of the river, then through the river mouth and up to the offshore limit of the turbid plume (see the detailed transect as black crosses on Figure 7A (top)). The SPM concentration is nearly constant (~50 g·m^{-3}) in the river and through the river mouth until the Mesurho station location then rapidly decreases (by a factor of 5) along a 15 km southward (offshore) distance. It then remains rather stable and constant (~10 g·m^{-3}) up to the limits of the plume before sharply decreasing again down to a minimum value of about 2 g·m^{-3} 40 km offshore. Based on Figure 7A, the 250 m MODIS-like resolution should also be able to estimate SPM concentrations in the downstream part of the Rhône River. Most of the details observed at 30 m resolution are still visible at this resolution, but progressively disappear until a resolution of 1 km. At the 1 km resolution, the river mouth is represented by only a few pixels and small-scale features are lost, but major patterns are preserved and SPM concentration ranges in the plume and river mouth are still consistent with higher spatial resolution observations. The 3×5 km^2 coarse spatial resolution of SEVIRI allows to globally map the extension and shape of the river plume so as the decrease of SPM concentrations from the mouth to offshore waters. However, turbidity front contours are lost and replaced by coarse boundaries. The river mouth as well as the secondary plume in front of the "petit Rhône" river mouth are still detected but are represented by only two or three pixels with SPM concentrations significantly lower than those observed at higher spatial resolution.

The accuracy and reliability of SPM concentrations estimated from meter to kilometer scales will depend on the spatial resolution but also on the SPM concentration spatial variability within the dimensions of the satellite pixel. The spatial variability of SPM concentrations at OLI native resolution within coarser pixels is illustrated in Figure 7B by standard deviation maps and density scatterplots. As expected, the coarser is the satellite spatial resolution the higher is the spatial variability of SPM concentration (as illustrated by the increase of vertical striping on the density scatter plots (Figure 7B)). However, standard deviation maps show that this variability is not constant throughout the river plume. The highest spatial variability is observed in plume edges, especially in northeastern and northwestern edges, as well as in intermediate turbidity fronts. These areas are characterized by a strong SPM concentration gradient mainly due to a fast concentration decrease. On the northeastern and northwestern edges, the SPM concentration can drastically decrease within a few kilometers distance (e.g., ~40 g·m^{-3} in less than 5 km, Figure 7A). In intermediate turbidity fronts, the decrease in SPM concentration is lower than in the edges but is still well represented by strong slopes on the OLI SPM concentration transect (Figure 7C). In low turbid waters (*i.e.*, mainly outer plume waters), the SPM concentration is rather constant resulting in a mean variability (values from standard deviation maps) lower than 2 g·m^{-3} at all spatial resolutions and a maximum variability (maximum minus minimum SPM concentrations at OLI spatial resolution within coarser satellite pixels (see scatter plots on Figure 7B)) lower than ~3 g·m^{-3}. In the turbid waters of the river plume, the SPM concentration mean variability within aggregated pixels progressively increases from ~1 g·m^{-3} at a resolution of 250 m to ~3 g·m^{-3} at a 1 km resolution (with a corresponding maximum variability of ~2 and ~5 g·m^{-3}, respectively). In the northeastern and northwestern edges of the plume, the mean variability of SPM concentration can reach ~7 g·m^{-3} and ~10 g·m^{-3} for spatial resolutions of 250 m and 1 km respectively, with a corresponding maximum variability of ~10 and ~30 g·m^{-3}. Within SEVIRI-like simulated pixels, the mean variability of SPM concentrations is lower than ~5 g·m^{-3} over the river plume but increases to 6–12 g·m^{-3} in edges and at the river mouth. The corresponding maximum

variability reaches values as high as ~17 g·m^{-3} near the mouth and even 40 g·m^{-3} in the plume Northern edges. This is consistent with the strong decrease of SPM concentrations observed along a distance of 5 km using OLI data (Figure 7C). Inside the SEVIRI-like pixel, highest values of SPM concentrations at the river mouth are averaged with lower values present offshore (Figure 7B,C), which results in the observed lower SPM concentration values and higher variability of SEVIRI-like pixels compared to other resolutions.
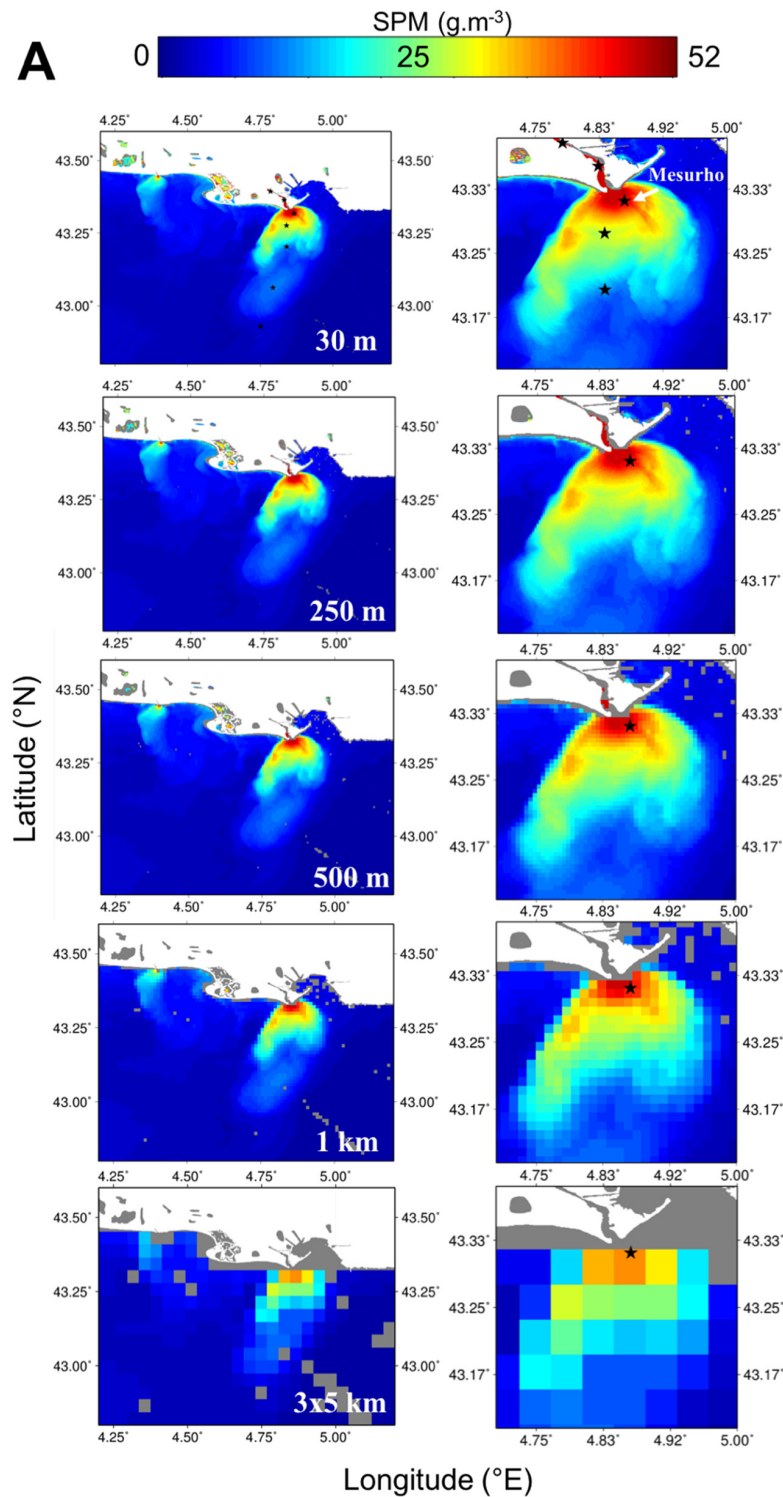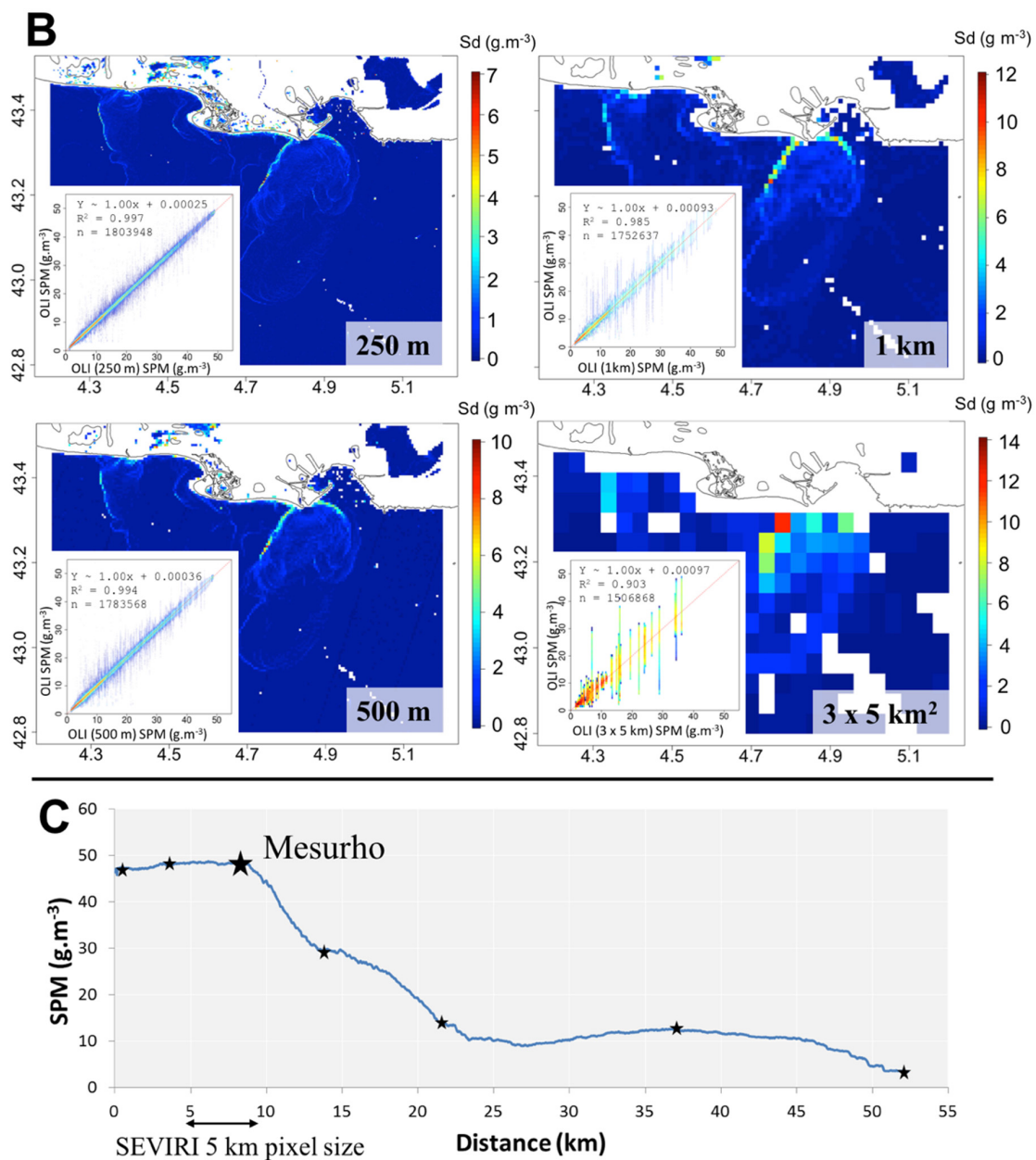

Figure 7. *Cont.*

Figure 7. (**A**) Full OLI image of SPM concentration over the Rhône River plume (left) and zoom on the Rhône River mouth (right) at the OLI native resolution (30 m) (top). Then averaged into coarser grids of 250 m, 500 m, 1 km and 3 × 5 km, from top to bottom row, corresponding to MODIS and SEVIRI resolutions. SPM concentrations are obtained using Rrs *vs.* SPM concentration relationship obtained in Section 3.1.1; (**B**) Maps of the standard deviation of SPM concentration at OLI native resolution (30 m) into aggregated pixels. Color scales are adapted to each map and illustrated with color bar. In order to better illustrate the whole variability of OLI SPM concentration into aggregated pixels, scatter-plots of OLI data at native resolution (30 m) as function of the resampled data are also presented. The color on the scatter plots denotes pixel density; (**C**) SPM concentration profile derived from the OLI native resolution image, as a function of distance from the mouth. Path used for this profile is illustrated by black stars on two OLI native resolution images in (**A**).

These results suggest that a spatial resolution up to 1 km is suitable to retrieve consistent SPM concentration values near the river mouth and along the river plume, except for some regions showing strong SPM concentration gradients mainly localized in intermediate turbidity fronts and plume

edges. SEVIRI should be able to globally reproduce the plume shape and extension and retrieve SPM concentration ranges. However, the high variability observed inside a SEVIRI-like pixel may prevent to quantitatively compare SEVIRI-derived Rrs and SPM concentration values with satellite or *in situ* higher spatial resolution data, as it will be either over or underestimated, depending on the reference data position (any high resolution sensors pixel or *in situ* measurements) in the SEVIRI-like pixel.

### 3.2.2. Comparisons between True OLI, MODIS and SEVIRI SPM Products

A comparison between observations of the Rhône River plume using OLI (30 m), MODIS-A and MODIS-T (250 m) and SEVIRI (3 × 5 km^2) is shown in Figure 8. The four images were recorded on 23 February 2014 at 10:24, 13:10, 09:50 and 09:45 UTC respectively. The MODIS-T image shows an overall low quality because of the location of the Rhône River plume at the border of the MODIS-T swath. As predicted in the previous section, OLI (30 m) and MODIS (250 m) resolutions well reproduce the plume extension and small-scale turbidity features. OLI spatial resolution allows observing SPM concentration upstream the river mouth, but this part is flagged as clouds and/or saturated pixels during the l2gen processing of MODIS-A and -T images. Rrs and SPM concentrations products at OLI and MODIS (250 m) spatial resolutions are globally consistent, with SPM concentrations ranging from ~10 g·m^{-3} in the offshore part of the plume to ~40 g·m^{-3} near the mouth. Note that the MODIS-T SPM product shows slightly lower SPM concentrations in the river mouth. This can be explained by either the natural variability of the water turbidity between MODIS-T and OLI acquisition times (35 minutes) and/or by the systematic underestimation of Rrs values by MODIS-T compared to OLI and MODIS-A (see Section 3.1.2). Differences in the plume shape observed by OLI and MODIS-A can clearly be attributed to the natural plume dynamics between 10:24 and 13:10. As predicted, SPM concentrations observed with SEVIRI at a 3 × 5 km² resolution are globally lower than those estimated using OLI and MODIS. This is especially visible near the river mouth where SEVIRI-derived SPM concentrations do not exceed 30 g·m^{-3}. Note that these values are lower than those predicted by degrading the OLI resolution (Section 3.2.1). This can result from the systematic underestimation of Rrs by SEVIRI compared to other sensors (see Section 3.1.2) in addition to the effect of the low spatial resolution. Nevertheless, the global shape of the plume, composed here of two filament-like features, is preserved and the "petit Rhône" river plume is still visible with low SPM values.

3.2.3. Consistency between Rrs and SPM Concentrations at Meter (Field Measurements) and Kilometer (Satellite Data) Spatial Scales

Several match-ups between field and satellite data are available from the TUCPA oceanographic campaign: 4 for MODIS (2 with MODIS-A and 2 with MODIS-T) and 15 for SEVIRI. Unfortunately, there was no OLI image acquisition during the field campaign. The time difference between field measurements and MODIS and SEVIRI data is systematically lower than 11 minutes and most of them are lower than 5 min. The exact longitude and latitude recorded on the research vessel for each field measurement were used to select the corresponding pixel on MODIS and SEVIRI satellite images. The locations of the four match-ups identified with MODIS are reported on MODIS and SEVIRI images on Figure 9. The comparison between *in situ* Rrs (weighted by sensors sensitivity) and sensors estimated Rrs (Figure 10, left panel), shows that Rrs values derived from MODIS data are consistent with *in situ* Rrs measurement with an overall underestimation lower than 10% and a median relative difference of 7% (Figure 10A, left). Note that no difference in match-up quality is observed between MODIS-A and MODIS-T for these 4 match-ups. Considering the SPM concentration (Figure 10A, right), match-ups are consistent except for match-up 4 where the *in situ* SPM concentration is three times higher than that derived from MODIS (24 g·m^{-3} instead of 8 g·m^{-3}, respectively). Water turbidity for this match-up was measured during the field campaign using a portable HACH 2100Q and estimated at 5.2 FNU which is more consistent with the SPM concentration estimated by MODIS than with the *in situ* SPM concentration measurement. This suggests a measurement error during SPM filtration or weighing and leads us to discard this match-up. The three remaining match-ups show a rather good correspondence

with a slope close to 1 and a median relative difference lower than 6%. This confirms the capability of MODIS 250 m data to retrieve consistent Rrs and SPM concentration in the Rhône River plume and the validity of the atmospheric corrections applied.
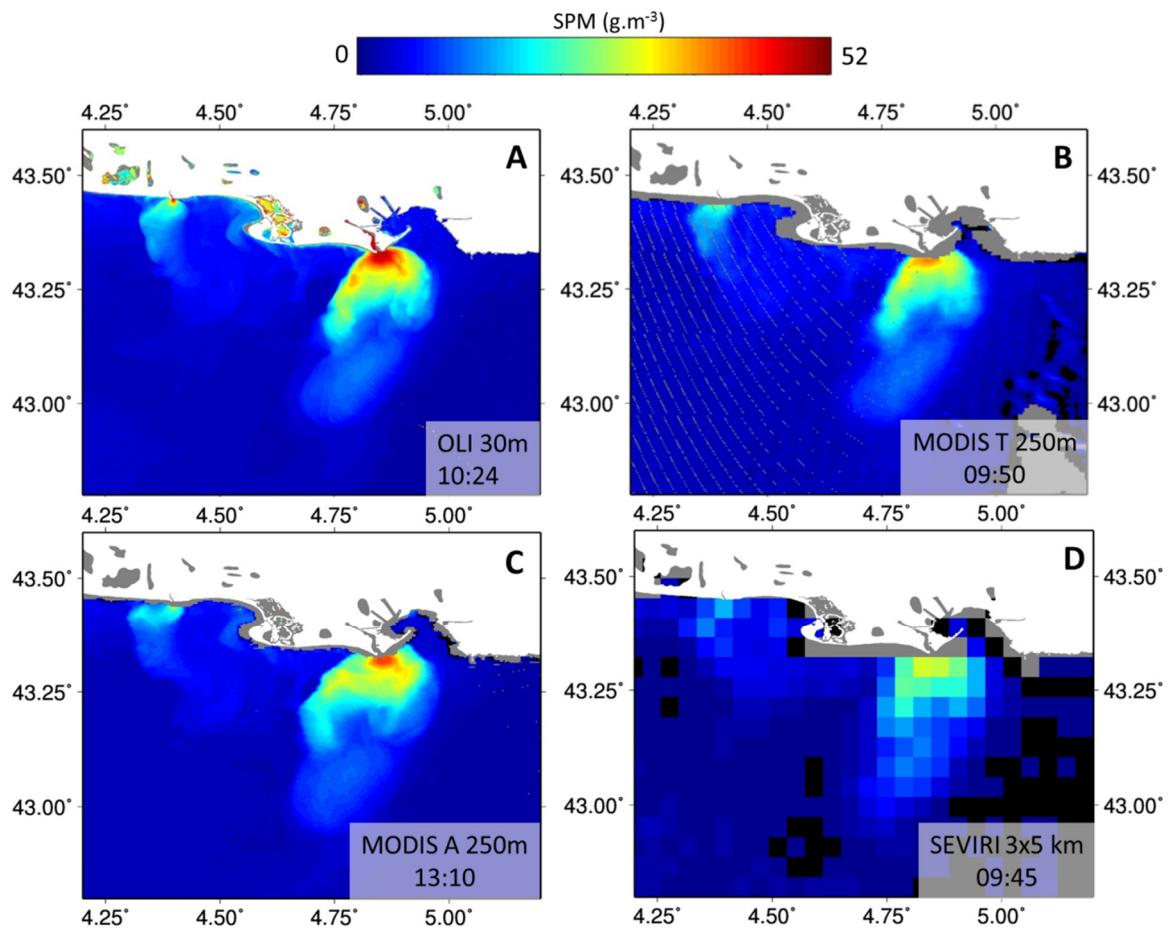
Figure 8. Satellite images of the SPM concentration over the Rhône River plume the 23rd February 2014. (**A**) OLI SPM product at 30m resolution acquired at 10:24; (**B**) MODIS-T and (**C**) MODIS-A SPM product at 250 m resolution acquired at 09:50 and 13:10 respectively and (**D**) SEVIRI SPM product at 3 × 5 km resolution acquired at 09:45. SPM concentrations are obtained using Rrs *vs.* SPM concentration relationship obtained in Section 3.1.1. Grey areas correspond to pixels masked by flags. The MODIS-T image (**B**) shows an overall low quality (*i.e.*, grey streak on left side) because of the location of the Rhône River plume at the border of the MODIS-T swath.
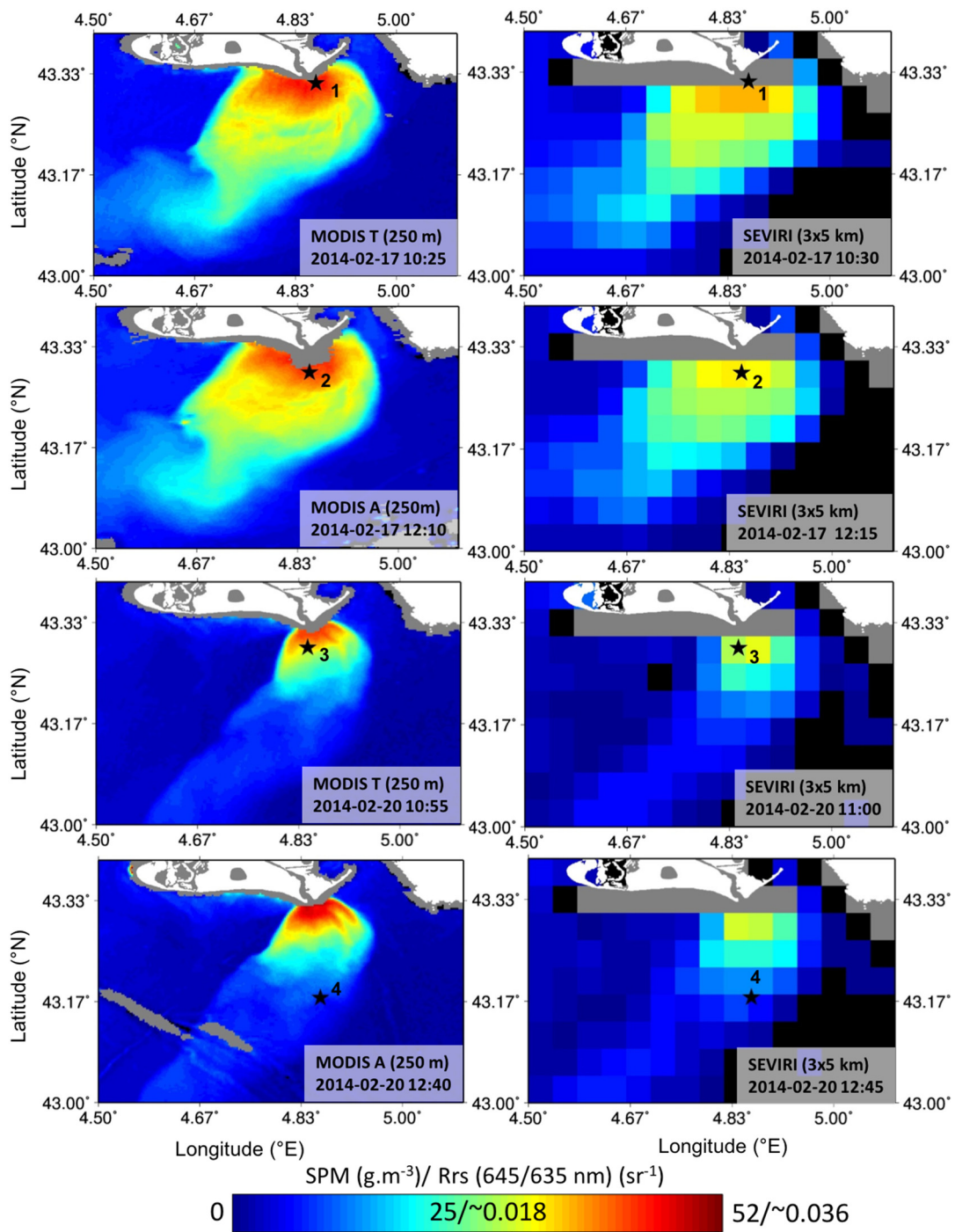
Figure 9. MODIS-A and -T SPM products (**left**) and SEVIRI SPM products (**right**) for the four match-ups identified with the TUCPA *in situ* data. Dates and times for the four match-ups are (1) 2014-02-17 10:24; (2) 2014-02-17 12:11, (3) 2014-02-20 11:07 and (4) 2014-02-20 12:51. More match-up are available with SEVIRI but are not shown here. In addition to SPM concentrations, corresponding Rrs values in the red band of the two sensors (645 nm for MODIS and 635 nm for SEVIRI) are also reported on the color scale.
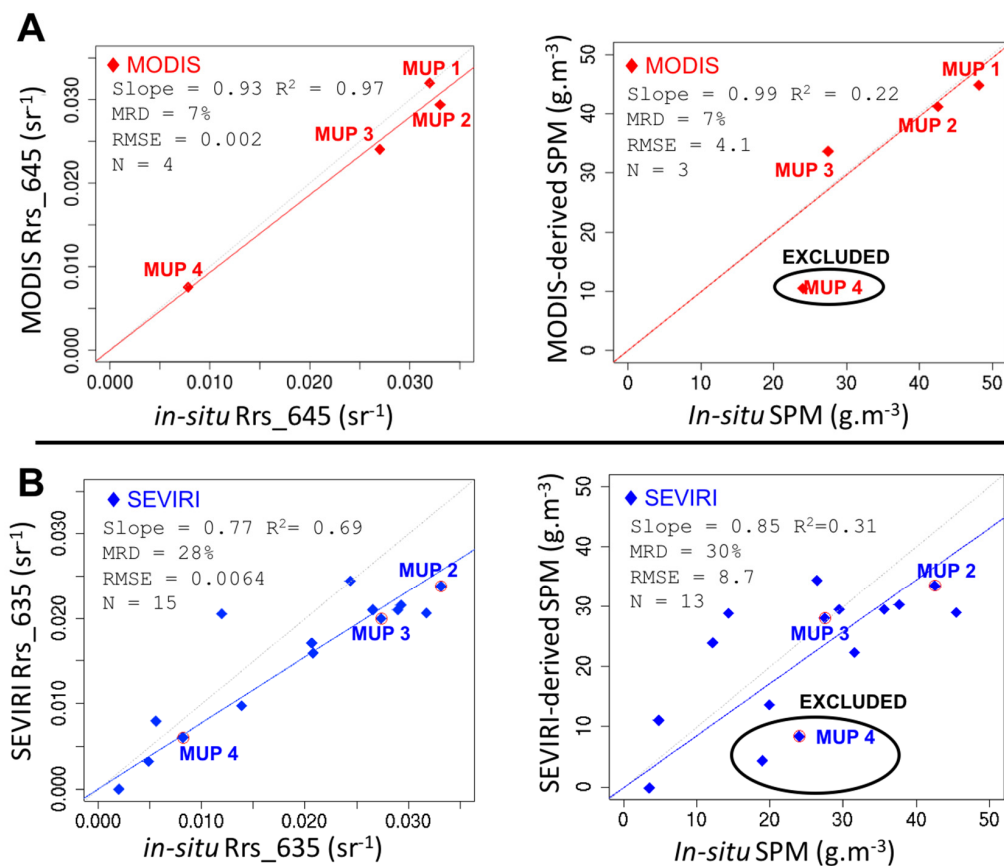
Figure 10. Comparison between (**A**) MODIS-A and -T and (**B**) SEVIRI derived Rrs (left) and SPM concentration (right) with *in situ* data from the TUCPA campaign. Linear regression are applied on each comparison. The R^2, median relative difference (MRD = median(| $DATA_{sensors}$-$DATA_{TUCPA}$ | / $DATA_{TUCPA}$*100)) and RMSE values are indicated. Some SPM concentration match-up were considered as not relevant because of *in situ* data measurement error (see Section 3.2.3) and were excluded.

As expected, differences between *in situ* and SEVIRI-derived Rrs for the 14 match-ups are higher than for MODIS (Figure 10B, left). Figure 10B shows that SEVIRI tends to underestimate Rrs by about 20% compared to *in situ* measurements. This is consistent with previous results based on comparison between satellite products and simulation of degraded spatial resolutions (Sections 3.1.2, 3.2.1 and 3.2.2). However, the correlation between SEVIRI-derived Rrs and *in situ* data is surprisingly good with a rather low dispersion (R^2 = 0.69). Note that the quality of match-up does not depend on SEVIRI data acquisition time (*i.e.*, of sun zenith angle) at least between 10:00 and 14:30. This comparison suggests that despite its low spatial resolution, SEVIRI is able to retrieve rather consistent Rrs values (at least between 10:00 and 14:30 at ~43°N), taking into account an underestimation of about 20%. This underestimation by SEVIRI compared to *in situ* data is lower for SPM concentration with an underestimation of about 15% (Figure 10B, right). However, the correlation between SEVIRI-derived and *in situ* SPM concentrations shows a significant scatter making difficult any reliable comparison between the SEVIRI SPM product and *in situ* SPM measurements (Figure 10B, right). This scatter is consistent with that observed in the Rrs *vs.* SPM concentration relationship established in Section 3.1.1 and mainly reflects the difficulties to link a punctual (in space and time) SPM sampling in the highly stratified Rhône River plume [8] to a SPM concentration derived from Rrs signal averaged over a kilometer scale area. On the contrary, *in situ* Rrs are acquired from above water and integrate the light backscattered by the potentially stratified surface waters over a meter scale area, making it a product more directly comparable to satellite-derived Rrs. These first results are encouraging and prove that the three satellite sensors spatial resolutions considered here (OLI 30 m, MODIS 250 m and

SEVIRI 3×5 km^2) can provide consistent and complementary observations of SPM concentrations in the Rhône River (downstream part), mouth and turbid plume.

3.3. Impact of Satellite Sensor Temporal Resolution on the Monitoring of SPM Dynamics

The Rhône River plume dynamics are typical of low tidal amplitude waters but can show strong hourly to monthly fluctuations in terms of SPM concentration, plume extent and orientation (e.g., [8,22–24]. The last step in the present study is to assess the potential of OLI, MODIS and SEVIRI satellite data to capture these SPM spatio-temporal dynamics in the river plume, *i.e.*, to test their capabilities in terms of temporal resolution to (1) estimate the variations of the flux of SPM at the river mouth and (2) observe the transport of SPM in the river plume.

3.3.1. Capabilities of SEVIRI and MODIS to Monitor the SPM Concentration Variations in the Rhône River Mouth Based on Field Data

Figure 11 shows hourly (Figure 11A) to daily (Figure 11B) variations of the SPM concentration derived from autonomous light backscattering measurements recorded at the Mesurho station close to the river mouth (see Section 2.2). Figure 11A focuses on hourly SPM concentration variations over the study period (17 to 23 February 2014). Measurements taken every 15 min are averaged over 1 h in order to keep only variations significant enough to be compared to variations observed from space at meter to kilometer spatial resolutions. These measurements show that despite a rather stable average value of ~60 g·m^{-3} over the study period, the SPM concentration at the river mouth shows high frequency fluctuations with hourly variations that can reach more than 100%. The acquisition time range of SEVIRI from ~08:00 UTC to ~16:00 UTC is represented by grey rectangles. The 15 min high temporal resolution of SEVIRI should allow following variations that occurred during this hourly range. However, as showed in Sections 3.2.1 and 3.2.3 its coarse pixel size makes difficult to make a reliable comparison between SEVIRI SPM products and *in situ* data. Moreover, the closest SEVIRI pixel from the coast is too far to see the Mesurho station location and points to the region localized just offshore where SPM concentration shows a strong decrease due to dilution and/or particle settling processes (Figure 7C). Despite its high temporal resolution, variations observed with SEVIRI are thus hardly comparable with *in situ* data recorded at the Mesurho station and cannot be used to describe the SPM concentration variations at the river mouth. The acquisition time of MODIS-T (~10:00 UTC) and MODIS-A (~13:00 UTC) are represented by vertical bars (respectively blue and red) on Figure 11A. The MODIS 250 m spatial resolution should allowed to follow small-scale spatial variations in the river mouth (Section 3.2.1.). However, Figure 11A shows that two MODIS images per day is not enough (and acquisition times of MODIS-A and -T data are too close) to describe the whole diurnal variability of the Rhône River plume. In order to simulate daily SPM concentration variations as observed by MODIS-A and MODIS-T, we report on Figure 11B the SPM concentrations measured by the probe at MODIS-A (red) and MODIS-T (blue) acquisition times for the period from the 22 January to 4 March. For comparison the daily averaged SPM concentration measured by the probe is also reported on Figure 11B. Accordingly to Figure 11A, the daily variations of SPM concentration as observed by the probe at MODIS-T and MODIS-A acquisition times show some differences due to hourly SPM concentration variations between the two acquisition times. Nevertheless, SPM concentrations measured at MODIS-T and MODIS-A acquisition times are globally consistent with daily averaged SPM concentrations and allow to follow day-to-day variations observed over the period. Based on these results, the temporal resolution of MODIS (*i.e.*, 2 images per day) is not sufficient to describe the high frequency SPM concentration variability in the Rhône River mouth highlighted by *in situ* probe data. However, it allows to monitor its daily to monthly SPM concentration dynamics. The SPM concentration variations as seen with the very low temporal resolution of OLI (yellow on Figure 11B) shows that this sensor cannot be used to estimate SPM fluxes at the river mouth.
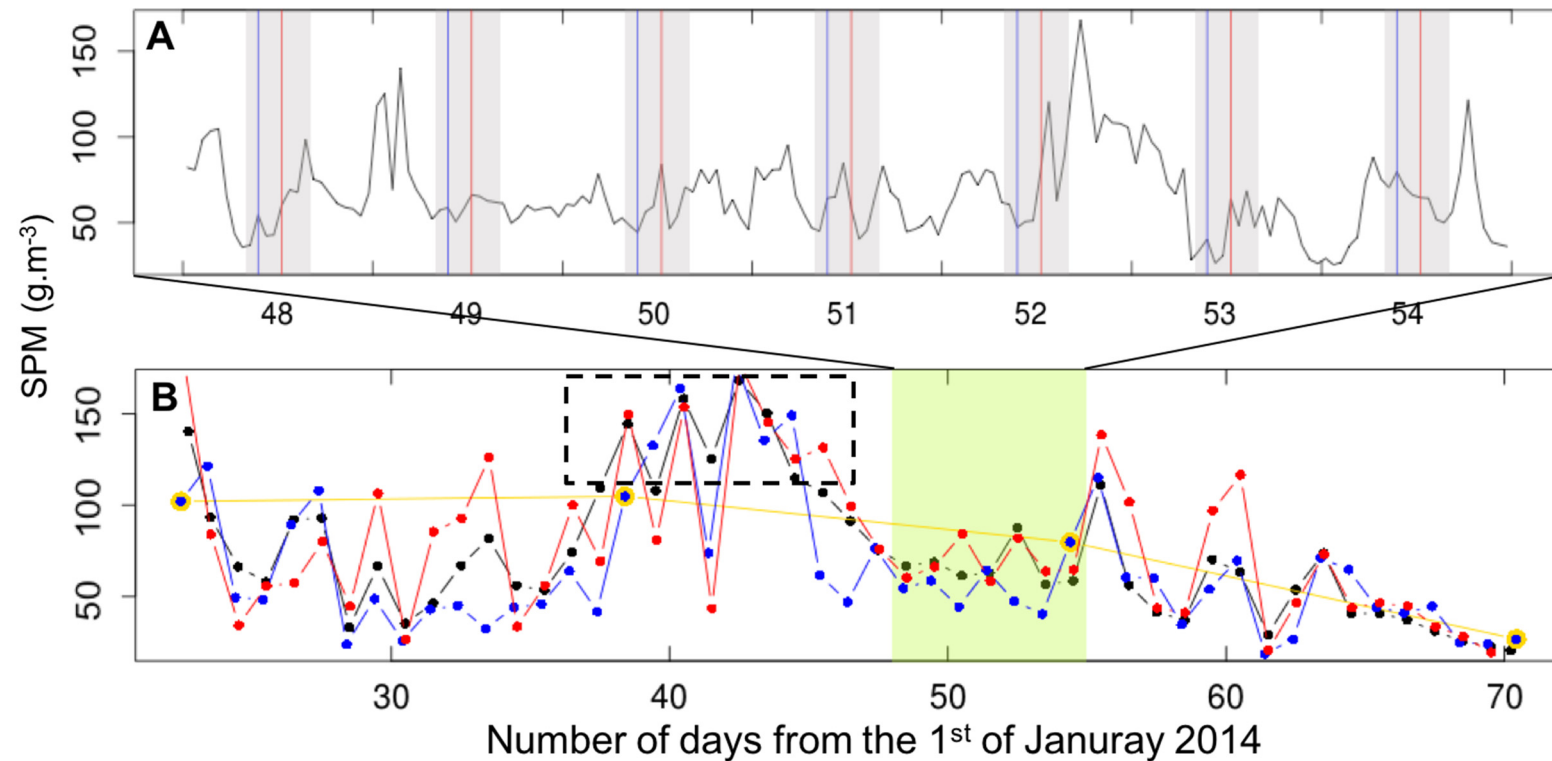
Figure 11. (**A**) SPM concentration variations in the river mouth over the studied period (17 to 23 February). SPM concentrations were computed from the particulate backscaterring coefficient $b_{bp}(700)$ measured by the Wetlabs ECO-BB2FL autonomous sensor mounted at the Mesurho station according to: SPM = $b_{bp}(700)$*F, with F = 416 a local calibration factor established using field measurements during the TUCPA campaign. SPM concentration measurements are averaged over 1h in order to keep only variation significant enough to be compared to variations observed from the space at meters to kilometers scales. The grey shaded regions correspond to the SEVIRI acquisition time range from 08:00 to 16:00 and the red and blue vertical line correspond to mean acquisition time of MODIS-A (10:00) and MODIS-T (13:00) respectively; (**B**) Daily averaged SPM concentration measured by the probe (black) over a large period ranging from 22 January to the 11 March 2014, compared to the SPM concentration measured by the probe at MODIS-A (red), MODIS-T (blue) and OLI (yellow) acquisition time. Dashed black rectangle indicates data that could be altered by probe saturation.

3.3.2. Capabilities of MODIS and SEVIRI Satellite Sensors to Map the Spatio-Temporal Dynamics of SPM in the Rhône River Plume

In addition to variations in SPM concentration, the extension of the Rhône River plume may show strong spatio-temporal dynamics mainly driven by coastal currents and winds (e.g., [22–24]). SEVIRI spatial resolution is not sufficient to observe small-scale turbidity features but allows to globally reproduce the shape, orientation and extension of the river plume. The hourly spatial dynamics of the plume observed with SEVIRI over the whole three day period covering the 17, 20 and 23rd February are illustrated on Figure 12 as contour lines along the 10 g·m^{-3} SPM concentration. The value of the 10 g·m^{-3} threshold is a compromise between integrating the largest part of the plume within the contour lines over the three days and preventing their disturbance by the noise present in clear waters. It allows to well follow the evolution of the moderate to high turbid part of the plume. This figure shows that the high temporal resolution of SEVIRI first provides an efficient monitoring of the spatial dynamics of the river plume. Significant diurnal and daily variations are observed during the three days. For comparison, the red contours correspond to plume boundaries (10 g·m^{-3}) derived from the MODIS-T (dashed line) and MODIS-A (solid line) images, degraded to the SEVIRI resolution. SEVIRI and MODIS-A and -T derived plume shapes observed at the same times are quite consistent. Some discrepancies can be observed between MODIS-A and SEVIRI, especially on the 17 February, which can be explained by the small underestimation of SPM concentration by SEVIRI compared to MODIS-A (see Section 3.1.2). Some variations in the plume shape, orientation and extension are observed between the MODIS-T and MODIS-A contour lines. However, Figure 12 shows that the two images per day provided by MODIS are insufficient to describe the whole hour-to-hour dynamics of the plume highlighted by SEVIRI, mainly because of the close time between MODIS-A and MODIS-T overpasses (no MODIS image recorded after 13:00 UTC). Nevertheless, over low cloud cover periods, MODIS data provide a high spatial resolution monitoring of the daily variations of the river plume. Over partly cloudy periods, the higher temporal resolution of SEVIRI increases the number of available images and thus significantly improves the monitoring of the plume dynamics.

Figure 12 illustrates the capabilities of SEVIRI and MODIS to capture the hourly and daily dynamics of SPM in the river plume during the study period. The decrease of the river freshwater discharge from the 17 to the 20 February (Figure 2) is clearly reflected in the extent of the turbid plume (as seen with the 10 g·m^{-3} SPM concentration line contours, *i.e.*, moderate to high turbid part of the plume). This extent significantly reduces over the four first days (17 to 20 February). Then, the river discharge shows a small increase during the 22 February that results in a well extended plume in the 23 February. Because of the Coriolis acceleration, the Rhône River plume naturally flows westward over the gulf of Lion, which is reinforced at the shelf edge due to the presence of the Northern Current. This is clearly observed with SEVIRI and MODIS SPM concentration contour lines (Figure 12). On the 17 and 20 February, the offshore part of the plume is extended toward the west, and for the three days, the whole plume is shifted from the east to the west during the day. Wind speed (Figure 12) was rather low during the study period (<10 m·s^{-1}) but wind direction showed high variability changing from south-west on 17 and 23 February to north-west on 20 February. Under a north-west wind, the plume is subject to a reverse effect of wind and sea stream, which results in a narrow plume, with a low SPM concentration offshore part that extends far to the south-southwest (see also Figure 9). Conversely, south-west wind pushes the plume toward the coast, which results in a larger and less extended plume. On 17 and 23 February, wind direction varied from the north-west to the south-west around 11:00 UTC. These wind conditions, associated to dilution and flocculation processes, likely explain the observed decrease of the plume extent after 14:00 UTC for these two days [53] (Figure 12). These short time variations (few hours) of plume shape under changing wind directions support a dominant and fast effect of wind stress on the river plume. These high frequency dynamics were already predicted by previous studies mainly based on modeling and *in situ* observations, and few satellite images (e.g., [8,17,22–24,57]). These dynamics were here observed and confirmed for the first time based on high temporal resolution satellite data such as those provided by SEVIRI.
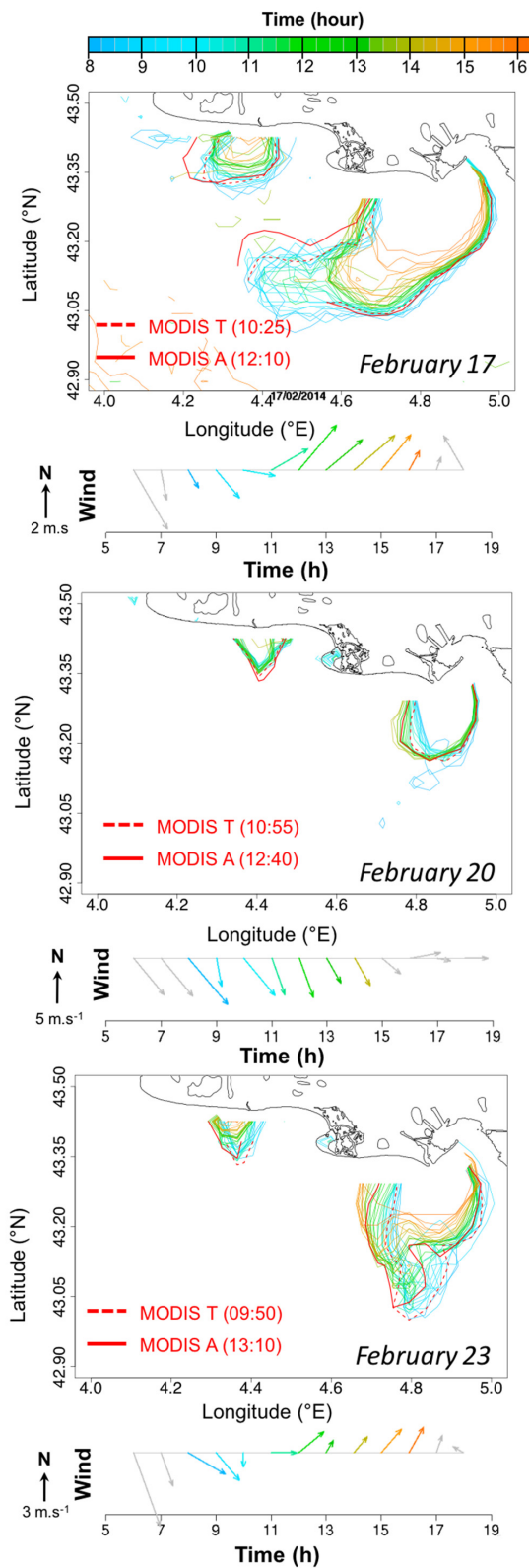
Figure 12. SPM concentration contour lines for concentration > 10 g m^{-3} derived from SEVIRI and MODIS-A and -T SPM product for the 17, 20 and 23 February 2014. SEVIRI contour lines for all images acquired every 15 min are mapped with color from blue (08:00) to yellow (16:00). MODIS-A and -T contour lines are mapped in red solid line and red dashed line respectively. For an easier comparison with SEVIRI, MODIS images are ressampled to the SEVIRI resolution. For comparison, the wind speed and direction for each hour (from 5:00 to 19:00 UTC) is also reported under each contour lines map with same color code as SEVIRI contours (grey arrows correspond to wind speed and direction for hours before and after SEVIRI and MODIS acquisition times).

4. Conclusions and Perspectives

The objective of this study was to assess the potential and limits of three complementary satellite radiometric sensors (namely OLI, MODIS and SEVIRI), in terms of spectral, spatial and temporal resolutions, to (1) retrieve consistent SPM concentrations and (2) monitor SPM dynamics in the moderately turbid waters of a river plume. The main results obtained are summarized hereafter:

1. Based on the water turbidity in the Rhône River plume, on sensor spectral bands availability and specifications, three different atmospheric corrections have been chosen for the three sensors: the SWIR correction for OLI [18], the MUMM correction for MODIS [37] and a MUMM-based atmospheric correction for SEVIRI [19,20] using its red and NIR bands (MUMM-S). These three corrections are suitable for the moderately turbid waters of the Rhône River plume but the MUMM-based corrections have to be taken with caution in the most turbid waters of this study area (Rrs > ~0.025 sr^{-1}, SPM > ~35 g·m^{-3}).

2. The red band of the three sensors is the most appropriate to accurately estimate the SPM concentration in moderately turbid waters where SPM concentrations typically vary from about 5 to 60 g·m^{-3}. A simple linear relationship allows inverting Rrs into SPM concentration in such coastal waters.

3. Despite differences in data processing (mainly atmospheric corrections), waveband ranges and radiometric characteristics, the three sensors tested provide consistent Rrs values in the red spectral region in such moderately turbid waters (Rrs > 0.01 sr^{-1}). A maximum difference of ~16% (median value) was observed between SEVIRI and MODIS-A, as already reported for the southern North Sea [12]. This difference is lower between SEVIRI and MODIS-T (~6%). For the highest Rrs values (> 0.023 sr^{-1}), rather high differences were also observed between OLI and MODIS-A (9%) and -T (16%). They are mainly attributed to an underestimation of Rrs in the most turbid waters due to the MUMM atmospheric correction.

4. The high spatial resolution of OLI provides impressive details in terms of small-scale turbidity features. It allows mapping surface SPM concentrations along a continuum formed by the river itself (downstream part), the river mouth and the whole river plume up to its offshore limits. This should allow better understanding the transport and fate of terrestrial particles exported by rivers into the coastal ocean. The details of turbidity features are progressively lost using 250 m, 500 m and 1 km MODIS spatial resolution data. However, the surface SPM concentration estimates at the mouth and in the plume remain consistent. The mean variability of SPM concentrations within pixels is only ~1 and ~3 g·m^{-3} for spatial resolutions of 250 m and 1 km respectively (with a corresponding maximum variability of ~2 and ~5 g·m^{-3}, respectively). In regions of sharp SPM concentration variations, mainly turbidity fronts and edges, this mean variability increases to 7 and 10 g·m^{-3} for resolutions of 250 m and 1 km, ant the maximum variability can reach 10 and 30 g·m^{-3} respectively. The 250 m resolution of the MODIS red spectral band is thus sufficient and well appropriate to retrieve and map surface SPM concentration in the river mouth and in the plume. First comparisons between MODIS-derived Rrs and SPM concentration products with *in situ* measurements gave promising results. The coarse spatial resolution of SEVIRI prevents the monitoring of surface SPM concentration variations at the river mouth, where the variability of SPM concentration within the kilometer-size SEVIRI pixel can reach a mean value of 12 g·m^{-3} and a maximum value of 20 g·m^{-3}. It is nevertheless sufficient to reproduce the main shape pattern of the Rhône River plume and its SPM concentration range (taking into account an overall underestimation of about 15%–20% compared to higher resolution sensors and *in situ* data).

5. Despite the micro-tidal environment of the Rhône River plume, significant short-term (hourly) variations in its plume shape and SPM concentrations have been highlighted in this study. These high frequency dynamics were already predicted through modeling and *in situ* data, as well as using few satellite data, but was for the first time directly observed and confirmed through high temporal resolution satellite data such as those provided by SEVIRI. Indeed, SEVIRI

allowed highlighting significant diurnal variations of the plume shape, mainly controlled by river discharge, wind stress and regional circulation, and despite its low spatial resolution provides a suitable hourly to daily monitoring of the river plume dynamics. The two MODIS images per day occurrence allow to highlight trends in these hourly dynamics but only over a short time window (only 2 to 3 h) and before 13:00 UTC, which is not sufficient to reproduce the Rhône River plume dynamics over a whole day. Similarly, despite its high spatial resolution, the MODIS temporal resolution does not allow for the monitoring of high frequency (hourly) surface SPM concentration variations in the river mouth, highlighted by autonomous *in situ* probe data recorded at the Mesurho station. Nevertheless, MODIS temporal resolution is well adapted to monitor the daily dynamics of the plume shape and surface SPM concentrations. The low temporal resolution of OLI clearly prevents the monitoring of the dynamics of SPM in the Rhône River plume and the exploitation of its high spatial resolution for surface SPM fluxes estimation at the river mouth.

These results clearly highlight the complementarily of these three sensors and emphasize the advantage of a combination of multi-sensors data for the monitoring of river plumes. However, this monitoring is still limited by the low spatial resolution of SEVIRI and the low temporal resolution of MODIS and OLI data acquisitions. The next generation of polar-orbit satellite sensors, MSI onboard S-2 and OLCI onboard S-3, will provide data with a spatial resolution from 10 to 300 m and revisiting times from 5 to 1 day (respectively). In addition, the future Flexible Combined Imager (FCI) onboard the future geostationary satellite MTG-I will provide data with a spatial resolution of ~1 km and a higher revisiting time than SEVIRI (10 min). This new satellite sensors generation will allow developing new applications in coastal waters. These three sensors have red spectral bands suitable for SPM concentration retrieval, allowing their high frequency and high resolution monitoring in river plumes and coastal areas. As already observed with OLI in the Rhône River plume, the high resolution of MSI associated to its higher temporal resolution should allow following daily to weekly variations of SPM concentrations in the downstream part of the river. This should largely improve our current understanding of SPM transport and estimation of SPM discharge from the river into coastal waters through the river mouth. The combination of MODIS (or its successor), MSI, OLCI and OLI should permit the observation of fine turbidity features and turbidity front contours with higher spatial and temporal resolutions, allowing us to better observe and understand sediment transport in coastal waters (e.g., dilution of freshwater, settling of SPM, flocculation processes, *etc.*). This will provide valuable data for the calibration and validation of sediment transport and biogeochemical models. In addition to field measurements (buoys, gliders, floats, campaigns), it will help developing operational services for the monitoring of water quality in coastal areas, as well as for the optimization of dredging operation in ports and navigation routes [18]. In this study, we have shown that the 1 km spatial resolution of the future FCI should allow observing main turbidity features and retrieving consistent SPM concentrations in river plumes allowing a significant improvement of high frequency monitoring of river plume compared to the 3 × 5 km spatial resolution of SEVIRI. Since a few years, new methods were developed to merge multi-sensors ocean color satellite data in order to improve spatial and temporal resolution and coverage (e.g., [58]). First ocean color synergic products were developed for the southern North Sea [12] using MODIS and SEVIRI in order to combine their respective high spatial and temporal resolutions. These synergic products give improvement over both data sources with a good agreement with *in situ* data. This method was recently tested using simulated images of the new high-resolution satellite sensor OLCI and the future FCI [59], which should provide an unprecedented high resolution and high frequency monitoring of coastal waters. However, this synergic method assumes that the observed SPM concentration variability is mainly vertical (*i.e.*, resuspension of sediments from the seabed) and need to be adapted before being applied on river plumes mainly characterized by an horizontal variability (advective transport and dilution) such as the Rhône River plume.

In this study, valuable Rrs *vs.* SPM regional relationships were developed for the moderately turbid waters of the Rhône River plume. These relationships are based on an unprecedented dataset of *in situ* Rrs and SPM concentration measurements, as SPM concentrations as high as 60 g·m^{-3} were sampled for the first time, *i.e.*, not observed in previous campaigns [8]. However, it still needs to be improved with new *in situ* measurements in order to better constrain the inversion of low Rrs values as well as to confirm the linearity of this relationship. Recently, the TriOS-RAMSES hyperspectral radiometers were mounted on the Mesurho station in order to record autonomous Rrs measurements. Preliminary results are promising (already tens of quality match-ups with MODIS satellite data) for the validation of atmospheric corrections of satellite data. A fully equipped autonomous station (with radiometers and backscattering sensors) should permit, in the near future, a better validation of both atmospheric corrections and retrieval of SPM concentrations. Similarly, measurements from this autonomous station associated to new field campaign, notably at spring, should allow to develop and validate a regional relationship between Rrs and Chl-a concentration. Combination of multi-sensors dataset and validated regional relationship would finally provide an efficient monitoring of the annual to hourly SPM and Chl-a concentration dynamics in the Rhône River plume.

Author Contributions: Anouck ODY did the research work and wrote the paper; David Doxaran supervised the research work and the manuscript conception; Quinten Vanhellemont and Bouchra Nechad provided satellite data processing tools and their expertise on *in situ* radiometric data processing and algorithms. Stefani Novoa contributed to the data analysis and interpretation. Gaël Many, François Bourrin, Romaric Verney and Ivane Pairaud participated to the TUCPA campaign and provided gravimetric in situ data. They also provided their expertise about the Rhône River plume dynamics. Bernard Gentili provided *in situ* radiometric processing tools and its expertise on satellite data processing and formatting. All co-authors participated to the improvement of the manuscript.

Conflicts of Interest: The authors declare no conflict of interest

References

1. Schlunz, B.; Schneider, R.R. Transport of terrestrial organic carbon to the oceans by rivers: Re-estimating flux- and burial rates. *Int. J. Earth Sci.* **2000**, *88*, 599–606. [CrossRef]

2. Hedges, J.I.; Keil, R.G.; Benner, R. What happens to terrestrial organic matter in the ocean? *Org. Geochem.* **1997**, *27*, 195–212. [CrossRef]

3. Syvitski, J.P.M.; Peckham, S.D.; Hilberman, R.; Mulder, T. Predicting the terrestrial flux of sediment to the global ocean: a planetary perspective. *Sediment. Geol.* **2003**, *162*, 5–24. [CrossRef]

4. Stumpf, R.P.; Pennock, J.R. Calibration of a general optical equation for remote sensing of suspended sediments in a moderately turbid estuary. *J. Geophys. Res.* **1989**, *94*, 14363. [CrossRef]

5. Tassan, S. Local algorithms using SeaWiFS data for the retrieval of phytoplankton, pigments, suspended sediment, and yellow substance in coastal waters. *Appl. Opt.* **1994**, *33*, 2369–2378. [CrossRef] [PubMed]

6. Warrick, J.A.; Mertes, L.A.K.; Siegel, D.A.; Mackenzie, C. Estimating suspended sediment concentrations in turbid coastal waters of the Santa Barbara Channel with SeaWiFS. *Int. J. Remote Sens.* **2004**, *25*, 1995–2002. [CrossRef]

7. Miller, R.L.; McKee, B.A. Using MODIS Terra 250 m imagery to map concentrations of total suspended matter in coastal waters. *Remote Sens. Environ.* **2004**, *93*, 259–266. [CrossRef]

8.   Lorthiois, T.; Doxaran, D.; Chami, M. Daily and seasonal dynamics of suspended particles in the Rhône River plume based on remote sensing and field optical measurements. *Geo-Marine Lett.* **2012**, *32*, 89–101. [CrossRef]

9.   Gernez, P.; Lafon, V.; Lerouxel, A.; Curti, C.; Lubac, B.; Cerisier, S.; Barillé, L. Toward Sentinel-2 high resolution remote sensing of suspended particulate matter in very turbid waters: SPOT4 (Take5) Experiment in the Loire and Gironde Estuaries. *Remote Sens.* **2015**, *7*, 9507–9528. [CrossRef]

10.   Doxaran, D.; Froidefond, J.-M.; Castaing, P.; Babin, M. Dynamics of the turbidity maximum zone in a macrotidal estuary (the Gironde, France): Observations from field and MODIS satellite data. *Estuar. Coast. Shelf Sci.* **2009**, *81*, 321–332. [CrossRef]

11.   Doxaran, D.; Lamquin, N.; Park, Y.J.; Mazeran, C.; Ryu, J.H.; Wang, M.; Poteau, A. Retrieval of the seawater reflectance for suspended solids monitoring in the East China Sea using MODIS, MERIS and GOCI satellite data. *Remote Sens. Environ.* **2013**, *146*, 36–48. [CrossRef]

12.   Vanhellemont, Q.; Neukermans, G.; Ruddick, K. Synergy between polar-orbiting and geostationary sensors: Remote sensing of the ocean at high spatial and high temporal resolution. *Remote Sens. Environ.* **2013**, *146*, 49–62. [CrossRef]

13.   Vanhellemont, Q.; Ruddick, K. Turbid wakes associated with offshore wind turbines observed with Landsat 8. *Remote Sens. Environ.* **2014**, *145*, 105–115. [CrossRef]

14.   Doxaran, D.; Cherukuru, N.; Lavender, S.J. Apparent and inherent optical properties of turbid estuarine waters: Measurements, empirical quantification relationships, and modeling. *Appl. Opt.* **2006**, *45*, 2310–2324. [CrossRef] [PubMed]

15.   Nechad, B.; Ruddick, K.G.; Park, Y. Calibration and validation of a generic multisensor algorithm for mapping of total suspended matter in turbid waters. *Remote Sens. Environ.* **2010**, *114*, 854–866. [CrossRef]

16.   Doxaran, D.; Froidefond, J.M.; Lavender, S.; Castaing, P. Spectral signature of highly turbid waters: Application with SPOT data to quantify suspended particulate matter concentrations. *Remote Sens. Environ.* **2002**, *81*, 149–161. [CrossRef]

17.   Forget, P.; Ouillon, S. Surface suspended matter off the Rhone river mouth from visible satellite imagery. *Oceanol. Acta* **1998**, *21*, 739–749. [CrossRef]

18.   Vanhellemont, Q.; Ruddick, K. Advantages of high quality SWIR bands for ocean colour processing: Examples from Landsat-8. *Remote Sens. Environ.* **2015**, *161*, 89–106. [CrossRef]

19.   Neukermans, G.; Ruddick, K.; Bernard, E.; Ramon, D.; Nechad, B.; Deschamps, P.-Y. Mapping total suspended matter from geostationary satellites: a feasibility study with SEVIRI in the Southern North Sea. *Opt. Express* **2009**, *17*, 14029–14052. [CrossRef] [PubMed]

20.   Neukermans, G.; Ruddick, K.G.; Greenwood, N. Diurnal variability of turbidity and light attenuation in the southern North Sea from the SEVIRI geostationary sensor. *Remote Sens. Environ.* **2012**, *124*, 564–580. [CrossRef]

21.   Bourrin, F.; Durrieu de Madron, X.; Ludwig, W. Contribution of the study of coastal rivers and associated prodeltas to sediment supply in North-western Mediterranean Sea (Gulf of Lions). *Life Environ.* **2006**, *56*, 1–8.

22.   Broche, P.; Devenon, J.L.; Forget, P.; De Maistre, J.C.; Naudin, J.J.; Cauwet, G. Experimental study of the Rhone plume. Part I: Physics and dynamics. *Oceanol. Acta* **1998**, *21*, 725–738. [CrossRef]

23.   Estournel, C.; Kondrachoff, V.; Marsaleix, P.; Vehil, R. The plume of the Rhone: Numerical simulation and remote sensing. *Cont. Shelf Res.* **1997**, *17*, 899–924. [CrossRef]

24.   Estournel, C.; Broche, P.; Marsaleix, P.; Devenon, J.-L.; Auclair, F.; Vehil, R. The Rhone River Plume in unsteady conditions: Numerical and experimental results. *Estuar. Coast. Shelf Sci.* **2001**, *53*, 25–38. [CrossRef]

25.   Pont, D.; Simonnet, J.-P.; Walter, A.V. Medium-term changes in suspended sediment delivery to the ocean: Consequences of catchment heterogeneity and river management (Rhône River, France). *Estuar. Coast. Shelf Sci.* **2002**, *54*, 1–18. [CrossRef]

26.   Durrieu De Madron, X.; Abassi, A.; Heussner, S.; Monaco, A.; Aloisi, J.C.; Radakovitch, O.; Giresse, P.; Buscail, R.; Kerherve, P. Particulate matter and organic carbon budgets for the Gulf of Lions (NW Mediterranean). *Oceanol. Acta* **2000**, *23*, 717–730. [CrossRef]

27.   Ouillon, S.; Petrenko, A. Above-water measurements of reflectance and chlorophyll-a algorithms in the Gulf of Lions, NW Mediterranean Sea. *Opt. Express* **2005**, *13*, 2531–2548. [CrossRef] [PubMed]

28. Aloisi, J.C.; Cambon, J.P.; Carbonne, J.; Cauwet, G.; Millot, C.; Monaco, A.; Pauc, H. Origine et rôle du néphéloïde profond dans le transfert des particules au milieu marin. Application au Golf du Lion. *Ocean. Acta* **1982**, *5*, 481–491.

29. Boss, E.; Pegau, W.S. Relationship of light scattering at an angle in the backward direction to the backscattering coefficient. *Appl. Opt.* **2001**, *40*, 5503–5507. [CrossRef] [PubMed]

30. Pairaud, I.; Répécaud, C.; Ravel, M.; Fuchs, R.; Arnaud, M.; Champelovier, A.; Rabouille, C.; Bombled, B.; Toussaint, F.; Garcia, F.; *et al*. MesuRho: Plateforme instrumentée de suivi des paramètres environnementaux à l'embouchure du Rhône. In *Mesures Haute Résolution dans L'environnement Marin Côtier*; Schmitt, F.G., Lefebvre, A., Eds.; Presses du CNRS: Paris, France, 2015; in press.

31. Neukermans, G.; Loisel, H.; Mériaux, X.; Astoreca, R.; McKee, D. *In situ* variability of mass-specific beam attenuation and backscattering of marine particles with respect to particle size, density, and composition. *Limnol. Oceanogr.* **2012**, *57*, 124–144. [CrossRef]

32. Mobley, C.D. Estimation of the remote-sensing reflectance from above-surface measurements. *Appl. Opt.* **1999**, *38*, 7442–7455. [CrossRef] [PubMed]

33. Ruddick, K.G.; De Cauwer, V.; Park, Y.-J.; Moore, G. Seaborne measurements of near infrared water-leaving reflectance: The similarity spectrum for turbid waters. *Limnol. Oceanogr.* **2006**, *51*, 1167–1179. [CrossRef]

34. Aminot, A.; Kerouel, R. *Hydrologie des Ecosystèmes Marins: Paramètres et Analyses*; IFREMER: Brest, France, 2004.

35. Dogliotti, A.I.; Ruddick, K.G.; Nechad, B.; Doxaran, D.; Knaeps, E. A single algorithm to retrieve turbidity from remotely-sensed data in all coastal and estuarine waters. *Remote Sens. Environ.* **2015**, *156*, 157–168. [CrossRef]

36. Wang, M.; Shi, W. The NIR-SWIR combined atmospheric correction approach for MODIS ocean color data processing. *Opt. Express* **2007**, *15*, 15722–15733. [CrossRef] [PubMed]

37. Ruddick, K.; Ovidio, F.; Rijkeboer, M. Atmospheric correction of SeaWiFS imagery for turbid coastal and inland waters. *Appl. Opt.* **2000**, *39*, 897–912. [CrossRef] [PubMed]

38. Stumpf, R.P.; Arnone, R.A.; Gould, R.W.; Martinolich, P.M.; Ransibrahmanakhul, V. A partially coupled ocean-atmosphere model for retrieval of water-leaving radiance from SeaWiFS in coastal waters. In *SeaWiFS Postlaunch Technical Report Series*; Hooker, S.B., Firestone, E.R., Eds.; NASA Goddard Space Flight Center: Greenbelt, MD, USA, 2003; Volume 22, pp. 51–59.

39. Wang, M. Remote sensing of the ocean contributions from ultraviolet to near-infrared using the shortwave infrared bands: simulations. *Appl. Opt.* **2007**, *46*, 1535–1547. [CrossRef] [PubMed]

40. Wang, M.; Tang, J.; Shi, W. MODIS-derived ocean color products along the China east coastal region. *Geophys. Res. Lett.* **2007**, *34*, 1–5. [CrossRef]

41. Doron, M.; Bélanger, S.; Doxaran, D.; Babin, M. Spectral variations in the near-infrared ocean reflectance. *Remote Sens. Environ.* **2011**, *115*, 1617–1631. [CrossRef]

42. Wang, M.; Son, S.; Shi, W. Evaluation of MODIS SWIR and NIR-SWIR atmospheric correction algorithms using SeaBASS data. *Remote Sens. Environ.* **2009**, *113*, 635–644. [CrossRef]

43. Wang, M.; Shi, W. Sensor noise effects of the SWIR bands on MODIS-derived ocean color products. *IEEE Trans. Geosci. Remote Sens.* **2012**, *50*, 3280–3292. [CrossRef]

44. Irons, J.R.; Dwyer, J.L.; Barsi, J.A. The Next Landsat satellite: The Landsat data Continuity Mission. *Remote Sens. Environ.* **2012**, *122*, 11–21. [CrossRef]

45. Xiong, X.; Chiang, K.; Sun, J.; Barnes, W.L.; Guenther, B.; Salomonson, V.V. NASA EOS Terra and Aqua MODIS on-orbit performance. *Adv. Sp. Res.* **2009**, *43*, 413–422. [CrossRef]

46. Govaerts, Y.; Clerici, M. *MSG-1/SEVIRI Solar Channels Calibration Commissioning Activity*; Commissioning Activity Report EUM/MSG/TEN/04/0024; EUMETSAT: Darmstadt, Germany, 2004.

47. Shen, F.; Verhoef, W.; Zhou, Y.; Salama, M.S.; Liu, X. Satellite Estimates of wide-range suspended sediment concentrations in Changjiang (Yangtze) Estuary using MERIS data. *Estuaries Coasts* **2010**, *33*, 1420–1429. [CrossRef]

48. Knaeps, E.; Ruddick, K.G.; Doxaran, D.; Dogliotti, A.I.; Nechad, B.; Raymaekers, D.; Sterckx, S. A SWIR based algorithm to retrieve total suspended matter in extremely turbid waters. *Remote Sens. Environ.* **2015**, *168*, 66–79. [CrossRef]

49. Zhang, M.; Tang, J.; Dong, Q.; Song, Q.; Ding, J. Retrieval of total suspended matter concentration in the Yellow and East China Seas from MODIS imagery. *Remote Sens. Environ.* **2010**, *114*, 392–403. [CrossRef]

50. Binding, C.E.; Bowers, D.G.; Mitchelson-Jacob, E.G. Estimating suspended sediment concentrations from ocean colour measurements in moderately turbid waters; The impact of variable particle scattering properties. *Remote Sens. Environ.* **2005**, *94*, 373–383. [CrossRef]

51. Morel, A.; Gentili, B. Diffuse reflectance of oceanic waters. 3. Implication of bidirectionality for the remote-sensing problem. *Appl. Opt.* **1996**, *35*, 4850–4862. [CrossRef] [PubMed]

52. Gordon, H.R.; Brown, O.B.; Jacobs, M.M. Computed relationships between the inherent and apparent optical properties of a flat homogeneous ocean. *Appl. Opt.* **1975**, *14*, 417–427. [CrossRef] [PubMed]

53. Many, G.; Bourrin, F.; Durrieu de Madron, X.; Pairaud, I.; Gangloff, A.; Doxaran, D.; Ody, A.; Verney, R.; Menniti, C.; Le Berre, D.; Jacquet, M. Particle assemblage characterization in the Rhône River ROFI. *J. Mar. Sytems* **2016**, *157*, 39–51. [CrossRef]

54. Lorthiois, T. Dynamique des Matières en Suspension Dans le Panache du Rhône (Méditerranée Occidentale) par Télédétection Spatiale «Couleur de L'océan». Ph.D. Thesis, Université Pierre et Maris Curie, Paris, France, 2012.

55. Franz, B.A. Moderate Resolution Imaging Spectroradiometer on Terra: Limitations for ocean color applications. *J. Appl. Remote Sens.* **2008**, *2*, 023525. [CrossRef]

56. Loisel, H.; Morel, A. Non-isotropy of the upward-radiance field in typical coastal case 2 waters. *Int. J. Remote Sens.* **2001**, *22*, 275–295. [CrossRef]

57. Demarcq, H.; Wald, L. La dynamique superficielle du panache du Rhône d'après l'imagerie infrarouge satellitaire. *Ocean. Acta* **1984**, *7*, 159–162.

58. Aiken, J.; Gregg, W.; Kwiatkowska, E.; Maritorena, S.; Mélin, F.; Murakami, H.; Pinnock, S.; Pottier, C. Ocean-Colour Data Merging. In *Reports of the International Ocean-Colour Coordinating Group*; IOCCG: Dartmouth, NS, Canada, 2007; pp. 3–74.

59. Peschoud, C.; Minghelli-Roman, A.; Mathieu, S.; Lei, M. Study of the complementarity and the fusion of the future satellite sensors OLCI/Sentinel-3 and FCI/Meteosat Third Generation images. In Proceedings of IOCS Meeting, San Francisco, CA, USA, 15–18 June 2015.